MEE10:34

Fixed Receiver Bi-Static SAR Image Formation Using C/A code and Global Back-Projection Algorithm

Ahmed Hamza Ibrahim Makki

This thesis is presented as part of Degree of
Master of Science in Electrical Engineering

Blekinge Institute of Technology
May 2010

Blekinge Institute of Technology
School of Engineering
Department of Applied Signal Processing
Supervisor: Dr. Mats Pettersson
Examiner: Dr. Mats Pettersson

This page is left blank

Abstract

Synthetic Aperture Radar (SAR) is used to generate a high resolution radar image from low resolution aperture data. Different SAR configurations can be obtained. The research on the fixed receiver Bi-static SAR is still on its early stages and it is an interesting research hotspot. Bistatic SAR, spatially separated between the transmitter and receiver systems. The deployed transmitter determines the kind of the signals used with the SAR operations. The Coarse Acquisition (C/A) is one of the signals used in the Global Positioning System (GPS). It has a good correlation characteristics. The Global Back-Projection (GBP) algorithm is a time-domain imaging algorithm. The main advantages of GBP is that it can be used for wide bandwidth, unlimited scene size, perfect motion compensation, and it's ability to handle long integration angles. The algorithm however has one drawback which is the requirement of computation.

This work simulates in Matlab, fixed-receiver bistatic SAR image formation using C/A code and global back-projection algorithm, and comparing the performance with the monostatic configuration based on the obtained results. Also it analyzes the performance of different receiver locations in bi-static configuration.

Simulation results show that, the bistatic SAR range resolution strongly depends on the receiver location. The best resolution is obtained when the receiver is located between the transmitter and the target. In the best case, the azimuth resolution of the bistatic SAR is twice of the monostatic case while the range resolution is almost the same.

Keywords: Bi-static SAR, monostatic SAR, GBP, C/A code.

This page is left blank

Acknowledgments

All thanks to ALLAH, the most merciful, beneficent and the most gracious, who provided me guidance, strength and ability to complete this work.

I would like to thank Dr. Mats Pettersson for giving me the opportunity to do work on such a wonderful topic, and for his constant support and guidance through the research work, without his help and expert guidance, this thesis would have never been finished.

I would also like to thank Vu Viet Thuy for his help and support during this work.

In addition, I would like to thank BTH staff for giving me the opportunity to join such a program.

Special thanks to my friends and colleagues who made the life easy for me.

Finally, I want to express my hearty gratitude to my family for their continuous encouragement, support, and for their love.

Ahmed Hamza

Karlskrona

May,2010

This page is left blank

Table of Contents

This page is left blank

List of Figures

This page is left blank

List of Tables

This page is left blank

CHAPTER 1

Introduction

1.1 Introduction

Synthetic Aperture Radar (SAR) is used to generate a high resolution radar image from low resolution aperture data. The main purpose of SAR is to improve the azimuth resolution, but in indirect way, it helps to improve the range resolution as well. Different SAR configurations can be obtained such as monostatic configuration and bistatic configuration. Bistatic SAR, spatially separated between the transmitter and receiver systems while in monostatic case they are co-located. The Coarse Acquisition (C/A) code is one of the signals used in the Global Positioning System (GPS). It has a good correlation characteristics. There are two classes of SAR imaging algorithms, frequency domain algorithms and time domain algorithms. Global Back-Projection (GBP) algorithm is a time-domain algorithm. It is a point-by-point reconstruction method. The main advantages of GBP that it can be used for wide bandwidth, unlimited scene size, perfect motion compensation, and ability to handle long integration angles while the relative drawback, they require heavy computational load.

The research on the fixed receiver Bi-static SAR is still on its early stages and it is an interesting hot research area. Bi-static SAR has several merits compared to monostatic SAR such as, increasing system survival, obtaining different object scatter information, and improving stealth in detectability. Also it can utilize the existing active space-borne systems such as GPS satellites as non-dedicated transmitting sources which provide cost-effective imaging system and the possibility of frequent updates.

1.2 Thesis Scope

The aim of this work is to study the fixed-receiver bistatic SAR image formation using C/A code and global back-projection algorithm, and comparing the performance with the monostatic case based on the results obtained using a MATLAB simulation. Also different receiver locations will be taken into account to determine the best position for the receiver.

1.3 Thesis Outlines

The next chapter, chapter 2, gives an overview of the GPS which includes in details the description of the C/A code which will be used along with this work.

Chapter 3 describes the RADAR and SAR fundamentals, it also describes some concepts related to the SAR system.

Chapter 4 gives an introduction to the SAR data processing algorithms. It also gives an overview of the GBP and describes the principle of working.

Chapter 5 describes the simulated setup and the assumptions made in the simulations. In this chapter the simulation results are presented.

Finally chapter 6 presents the conclusions and recommendations for future work.

CHAPTER 2

Global Positioning System (GPS)

2.1 Introduction

The development of satellite systems for three dimensional position and time information with the optimal requirements such as global coverage (anywhere, anytime (continuous)), under any condition (clouds, rains, sun, etc), and with high accuracy started in the early 1960s at the Department of Defense (DOD) and the National Aeronautics and Space Administration (NASA) [1].

The Global Positioning System (GPS) was developed by DOD in the early 1970s. Although it is a Global Navigation Satellite System (GNSS) which was mainly developed for military purposes, the GPS has been widely used in several civilian applications and now it can be accessed by civilians as well as military people [1] - [3]. The following paragraphs describe the GPS.

2.2 GPS Overview

The GPS consists of three main parts: space segment, control segment, and the user segment. The following paragraphs give a general description to these three segments.

2.2.1 Space Segment

The space segment consists of a minimum of 24 GPS satellite distributed in six earth-centered orbital planes with four GPS satellite in each plane [1]. The orbits are Semi-circular with orbital radius of 26,600km and inclination of 55^{o} .The orbital period is 11 hours,58 minutes and 2 sec [1][3].

The operating GPS satellites transmit signals that provide the positioning and timing information in addition to information about data, status, and corrected orbit parameters [1].

2.2.2 Control Segment

The control segment ensures that the satellites are working properly. It consists of a Master Control Station (MCS) which is responsible of the system operation, provision

of commands, and control functions for the satellite constellation and a six worldwide monitor stations to continuously track the satellites [3].

2.2.3 User Segment

The user segment consists of the GPS receiver equipment, which capture and process the signals from the GPS satellites in view to calculate the user's position, time and velocity [3]. To do this, at least four satellite signals should be processed by the receiver.

2.3 GPS Signal Structure

The GPS signal is combination of carrier wave, coarse / acquisition (C/A) code, P-code, and navigation message. The carrier waves generally involve L1 and L2 bands [1][2]. The different parts are briefly explained in the next paragraphs while C/A code is described in more details.

2.3.1 Coarse Acquisition (C/A) Code

The Coarse Acquisition (C/A) code is also called Pseudo-Random Number (PRN) code which is a succession of ones and zeros. The bandwidth of the C/A code is $B = 2.046\ MHz$ [4]. Every satellite is assigned to a unique PRN code. Depending on which PRN code is assigned to a particular satellite, PRN code or number is given to that satellite, i.e. a satellite is named as PRN-1, if the PRN (C/A) code 1 is assigned to that satellite [2].

There are about 37 C/A codes; the first 32 C/A codes are used in the space segments while the rest (five codes) are reserved for other uses [1]. The C/A code is 1 ms long and this due to the code length is 1023 and the frequency of the C/A code is 1.023 MHz so the repetition period is (1023/ (1.023*10^6 Hz) =1ms).

The main characteristic of C/A codes is that they have the best correlation characteristic .i.e. the auto-correlation of each of the codes is much higher compared to the cross-correlation with any other code, also they are easy to generate but the synchronization is more difficult [2] .

2.3.1.1 C/A code Generation

The C/A code generator is presented in Fig. 2.1. There are two shift registers (G1 and G2), each one has a length of 10 $bits$ and these are used to generate a PRN code of length $N=2^{10}-1=1023\ bits$ (all zeros state is the only not used state). A unique C/A code is generated using the two PRN codes. The output of the second generator (G2) is delayed then combined by an exclusive-or circuit with the first generator (G1).

It is common to describe the design of linear code generators by means of polynomials of the form $1 + \Sigma X^i$, where X^i means that the output of the ith cell of the shift register is used as the input to the modulo-2 adder (exclusive-or), and the 1 means that the output of the adder is fed to the first cell.

For GPS The shift registers architecture is described by the following characteristic polynomials:

$$G1 = X^{10} + X^3 + 1$$

$$G2 = X^{10} + X^9 + X^8 + X^6 + X^3 + X^2 + 1$$

these polynomials describe the sequences and present the shift registers feedback used to generate the C/A code. The initial states of the individual register stages are ten ones (1111111111) at a time instant known as X1 epoch [1].

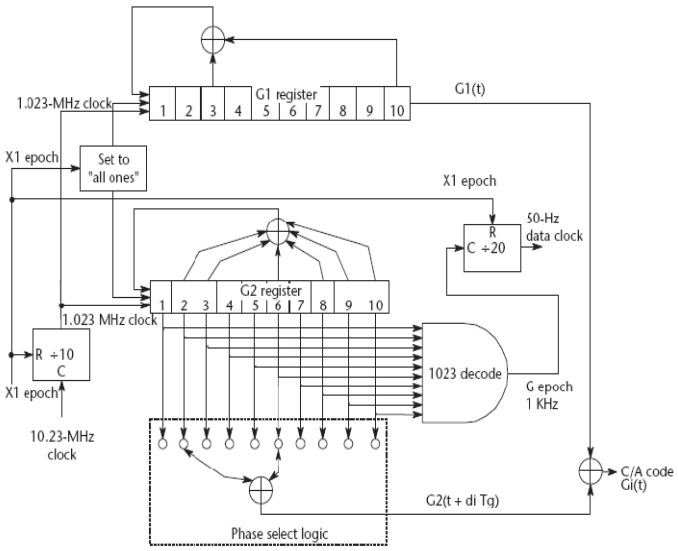

Fig. 2.1. C/A code generator [1]

2.3.1.2 C/A code correlation

The autocorrelation function is one of the greatest importance signal characteristics for the satellite navigation applications. The auto-correlation function for constant power low pass signal is given by

$$R(\tau) = \lim_{T\to\infty} \frac{1}{2T} \int_{-T}^{T} s^*(t)s(t+\tau)dt \qquad (2.1)$$

where * denotes complex conjugation.

As an example, the binary Direct Spread Spectrum Sequence (DSSS) signal shown in Fig.2.2 , has the autocorrelation function described by [1]

$$R(\tau) = \begin{cases} A^2\left(1 - \dfrac{|\tau|}{T_c}\right) & for\ |\tau| \le T_c \\ 0 & elsewhere \end{cases} \qquad (2.2)$$

wher A is the amplitude and T_c is the chip duration and it is illustrated in Fig. 2.3.

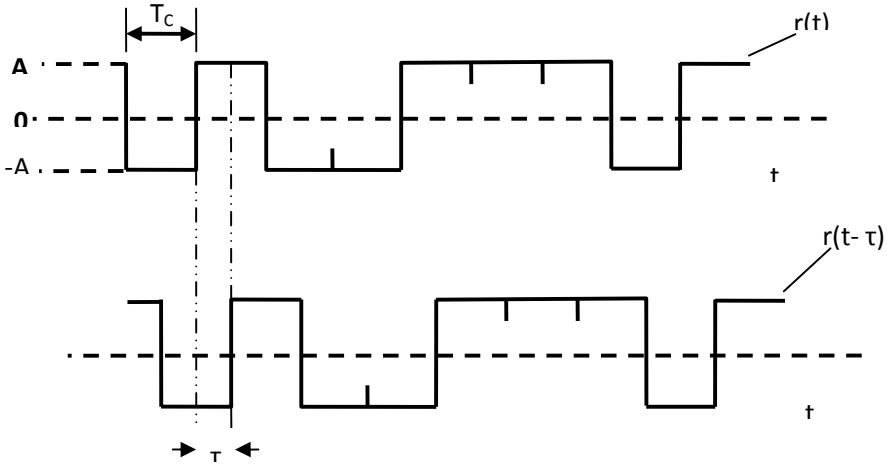

Fig. 2.2 Random binary code [1]

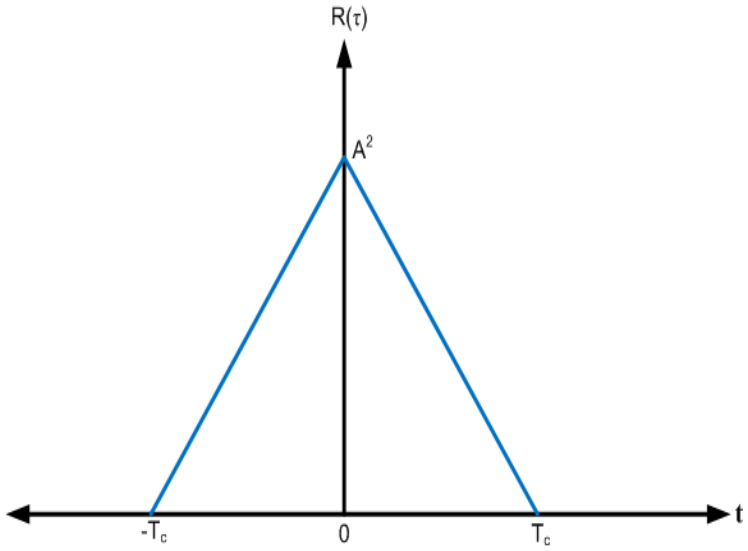

Fig. 2.3 The autocorrelation function for the random binary code.

The C/A codes correlation characteristics are interesting in this work; they have the best correlation characteristic .i.e. the cross-correlation of any two different codes is much lower compared to the auto-correlation of each of the codes. Fig. 2.4 shows the auto-correlation of PRN-1. The cross correlation between PRN-1 (C/A code 1) and PRN-2 (C/A code 2) is presented in Fig. 2.5. In this case, $T_c = 1/(1.023\ MHz) = 977\ ns$.

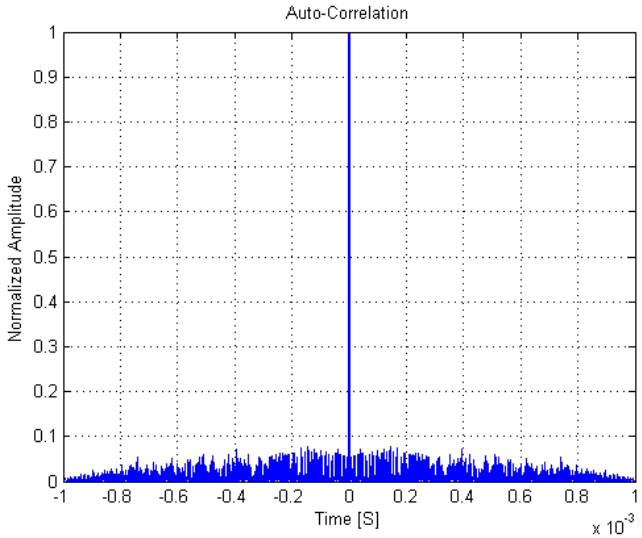

Fig. 2.4 Auto-correlation of PRN-1 C/A code.

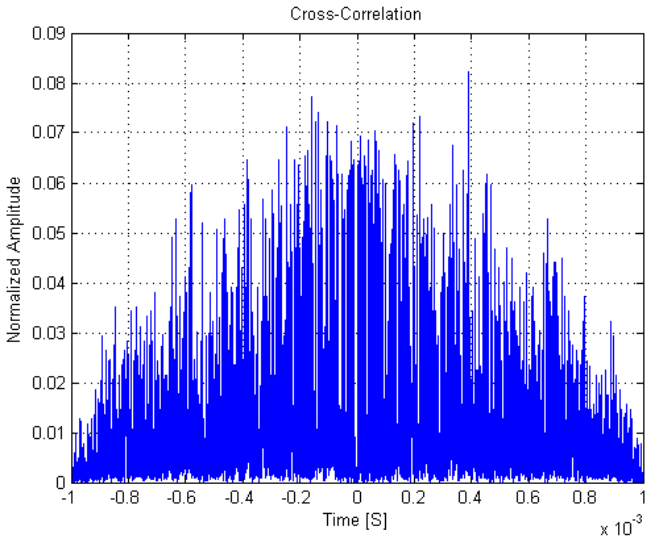

Fig. 2.5. Cross-correlation of PRN-1 and PRN-2 C/A codes. The cross-correlation is much lower compared to the auto-correlation of each of the codes.

2.3.2 P-Code

P-code consists also of zeros and ones and is generated using a set of Gold Codes. The Y-code is used to encrypt the P-code [2]. The frequency of P-code is 10.23 MHz and is generated using four 12-bit shift registers (X1A, X1B, X2A, and X2B). More details of the P-code generation and operation can be found in [1].

The initial states and the polynomials are presented in Table 2.1 for both P-code and C/A code generator shift registers [1] while a high-level block diagram for the two codes is depicted in Fig. 2.6.

Table 2.1 GPS Code Generator Polynomials and Initial States

Register	polynomial	Initial state
C/A code G1	$1 + X^3 + X^{10}$	1111111111
C/A code G2	$1 + X^2 + X^3 + X^6 + X^8 + X^9 + X^{10}$	1111111111
P code X1A	$1 + X^6 + X^8 + X^{11} + X^{12}$	001001001000
P code X1B	$1 + X^1 + X^2 + X^5 + X^8 + X^9 + X^{10} + X^{11} + X^{12}$	010101010100
P code X2A	$1 + X^1 + X^3 + X^4 + X^5 + X^7 + X^8 + X^9 + X^{10} + X^{11} + X^{12}$	100100100101
P code X2B	$1 + X^2 + X^3 + X^4 + X^8 + X^9 + X^{12}$	010101010100

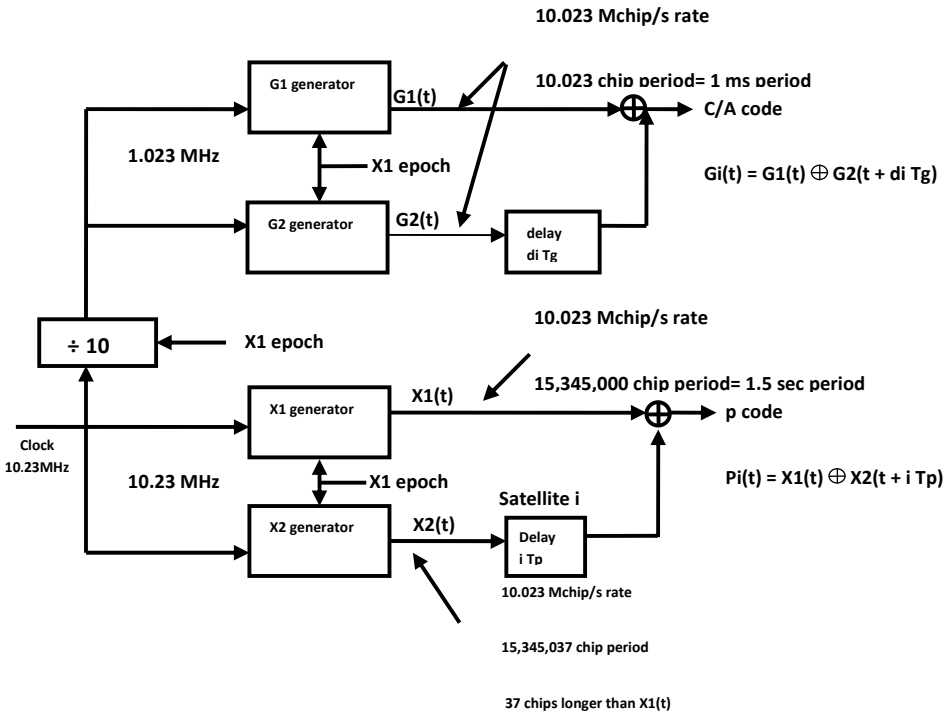

Fig. 2.6 GPS code generators [1]

2.3.3 Data Navigation

Navigation data consist also of zeros and ones, however they are based at a low rate which is 50 bits per second. The main use of navigation data is to send the information to the user from the satellite. Every satellite receives a message from the master control station which contains information about the state of the clock, the orbital parameters and another temporal data. More details can found in [1] and [4].

2.3.4 L1 band

The GPS L1 band center frequency is $f_1 = 1575.42\text{MHz}$ (wave length around 19 cm) which is derived from a fundamental frequency of $f_0 = 10.23\ \text{MHz}$ with a multiplication factor of 154, hence, $f_1 = 10.23 * 154 = 1575.42\text{MHz}$. L1 band has C/A code, P-code and navigation data [2] which can be given by

$$L1 = a_1 P(t) D(t) sin(\mathrm{f}_1 t + \Phi_{P1}) + a_1 C/A(t) D(t) cos(\mathrm{f}_1 t + \Phi_C). \qquad (2.3)$$

where a_1 is the amplitude, $P(t)$ is the P-code, $D(t)$ is the navigation data, Φ_{P1} is the phase error due to P-code, $C/A(t)$ is the C/A code , and Φ_C is the phase error due to C/A code.

Fig. 2.7 presents a general schematic to generate an L1 band signal as represented by the equation shown in the Fig. for C/A code [2].

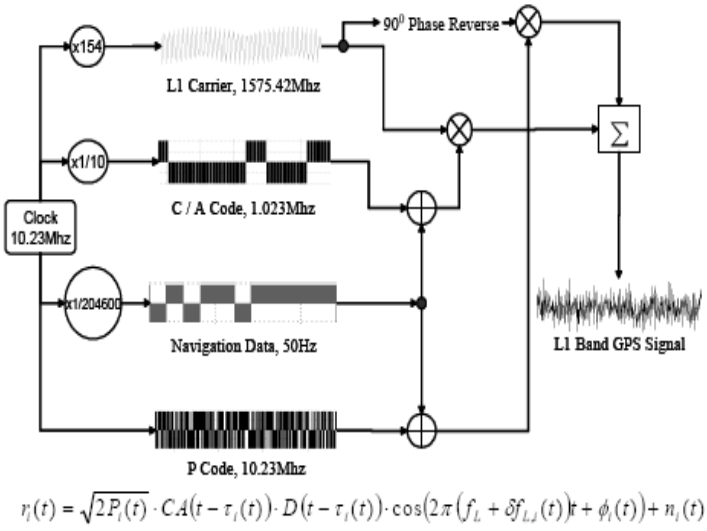

Fig. 2.7 Schematic showing the generation of L1 band GPS signal. The equation is the mathematical representation of C/A code in L1 band [2]

2.3.5 L2 band

The GPS $L2$ band center frequency is $\mathrm{f}_2 = 1227.60\mathrm{MHz}$ (wave length around $24\ cm$) which is derived from a fundamental frequency of $\mathrm{f}_0 = 10.23\ MHz$ with a multiplication factor of 120. $\mathrm{f}_2 = 10.23 * 120 = 1227.60\mathrm{MHz}$. L2 band has only P-code and navigation data [4] which is given by the following formula

$$L2 = a_2 P(t) D(t) sin(\mathrm{f}_2\, t + \Phi_{P2}). \qquad (2.4)$$

The $L2$ band and the encrypted P-code are used in military applications and the encryption codes are not accessible to the civilian community.

2.4 GPS Positioning Services

There are mainly two types of services, provided by the GPS system, which distinguish the military from the civilian use.

2.4.1 The Precise Positioning Service PPS

The PPS is primarily used in military applications since it predicts the positions with high accuracy. P-code in the two frequency bands (L1 and L2) is used with this service. The use of this service is only permitted to the authorized users [5].

2.4.2 The Standard Positioning Service SPS

The SPS is used in civilian applications and is free and available to all users worldwide. It is used to determine the positions with an acceptable accuracy using C/A code and L1 frequency band [5].

CHAPTER 3

Radio Detection and Ranging (RADAR)

3.1 Introduction

Radio Detection and Ranging is abbreviated as RADAR and it was originally developed for military purposes during World War II. It is an application of electromagnetic radio waves to detect targets and determine the target range [6]. Scottish scientist Robert Watson-Watt defined radar as follows - "Radar is the art of detecting by means of radio echoes the presence of objects, determining their direction and ranges, recognizing their character and employing data thus obtained in the performance of military, naval, or other operations."[7].

The principle of working is similar to the principles of measuring the distances by sound echoes but radio waves are used instead of sound. The system works by transmitting a radio pulse from the transmitter, this pulse reaches the target with a constant speed close to the speed of light; a part of this pulse will be reflected back to the RADAR receiver. The distance calculated by means of time and the velocity of propagation.

The RADAR can be classified according to the positions of the transmitter and receiver in the design of the system. RADAR in which the transmitter and receiver are separated is called Bistatic-RADAR; in other hand RADAR in which the transmitter and receiver are collocated is called Monostatic-RADAR.

The amount of power P_r returning to the receiving antenna is given by the radar equation for the Bistatic case

$$P_r = \frac{P_t \, G_t \, G_r \, \lambda^2 \sigma}{(4\pi)^3 \, R_t^2 R_r^2} \tag{3.1}$$

where P_t is the transmitting power, G_t is the gain of the transmitting antenna, G_r is the gain of the receiving antenna, σ is the radar cross section of the target, λ is the wave length, R_t is the distance from the transmitter to the target, R_r is the distance from the target to the receiver. Thus, the longer target radar cross section, the more energy will be reflected back to the receiver. In Monostatic-RADAR, both the transmitter and the

receiver at the same location, $R_t = R_r = R$, thus the equation of the radar is reduced to the expression

$$P_r = \frac{P_t G_t G_r \lambda^2 \sigma}{(4\pi)^3 R^4} \quad (3.2)$$

this shows that the received power declines as the fourth power of the range, meaning that the reflected power from distant targets is very small.

RADAR can be used in various applications such as meteorological detection of precipitation, measuring ocean surface waves, air traffic control, police traffic monitoring, and for military purposes.

Imaging RADAR provides a two dimensional image, one of the two dimensions is called the range and the other is called the azimuth. The range resolution is inversely proportional to the pulse bandwidth while the azimuth resolution can be improved when the antenna beam-width become smaller. Narrower beam-width requires a large antenna or higher frequency; however, there are practical limits for increasing the antenna length or the frequency[8].

3.2 Synthetic Aperture Radar (SAR)

In 1951, Carl wiley of the Goodyear Aircraft Corporation proposed an alternative means for improving the azimuth resolution. According to Carl, a pulse-to-pulse comparison of signals by a moving RADAR produces a finer azimuth resolution. This technique is known as Synthetic Aperture Radar (SAR). Hence, SAR is a coherent RADAR system which makes an image of the earth surface with high resolution. Normally the SAR system is installed in planes or space platform. In SAR there is a big antenna synthesized through the composition of successive and a coherent signal received as echoes from the signals transmitted by a smaller antenna along its flight track. The signal processing uses the magnitude and phase of the received signal of the different pulses in order to create the image [8]. With the movement of the antenna or real aperture through the different positions along the flight track the synthetic aperture is made.

3.2.1 Modes of SAR Operation

This section describes different modes of SAR operation which can be within a single system or it can be with different systems.

3.2.1.1 Stripmap SAR

In this mode of operation, antenna pointing is fixed relative to the flight line. The beam sweeps along the ground and a continuous image is formed. The antenna length limits the azimuth resolution [6][8].

3.2.1.2 *Scan SAR*

This mode is a variation of Stripmap SAR, the sensors steers the antenna beam to illuminate a strip of terrain at any angle to the path of motion. In this mode, a much wider swath is obtained with the cost of low azimuth resolution [6][8].

3.2.1.3 Spotlight SAR

In this mode, the sensor steers its antenna beam to continuously illuminate the terrain patch being imaged. Comparing this mode with Stripmap mode, the resolution is improved by increasing the angular extent of the illumination on the area of interest (a spot on the ground). In this mode of operation the coverage is not contiguous i.e. only one spot on the ground is imaged at a time[6][8].

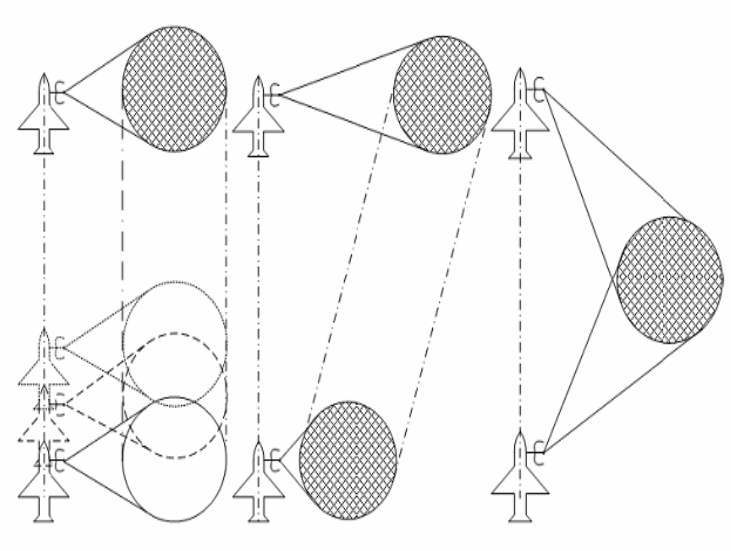

Fig. 3.1 SAR operation modes: stripmap, scan and spotlight [8]

3.2.1.4 Inverse SAR

In this case, the target is moving and the RADAR system is stationary. The signals are similar since the relative position and motion between the sensor and the scene being imaged is important. The processing required to produce an image is similar also. An example is the tracking of satellites from ground-based RADAR [6][8].

3.2.1.5 Bistatic SAR

In remote sensing SARs, the transmitter and the receiver are usually placed in the same location which is referred to as monostatic; if the transmitter and the receiver are at different locations, this mode of operation is called Bistatic [6]. In Space-Surface Bistatic SAR (S-SBSAR), the transmitter on a satellite while the receiver on the ground. The receiver consists of two subsystems: the heterodyne receiver for receiving the direct signal from the transmitter for signals synchronization and correlations, and the main receiver to receive the scatter from the target [9].

3.2.1.6 Interferometric SAR (InSAR)

In this mode of operation, post-processing is used to extract terrain height or displacement from the complex images [6].

3.3 SAR Geometry

Understanding the SAR operation used in this report needs a clarification to some terminologies and concepts which are defined in this section and illustrated in Fig. 3.2.

The basic element is a target, which is the part of the Earth's surface that the SAR system is imaging. A single representative point is considered when developing the SAR equations. This point is called "point target" or "point scatterer" or simply "target" or "scatterer". During the transmission of a particular pulse, the RADAR antenna projects a beam onto an area of the ground referred to as the beam footprint. The footprint is the part of the Earth's surface that is illuminated by the RADAR beam. The minimum range is the distance of the closest approach i.e. when the zero Doppler line crosses the target. It is denoted as R_0 . Zero Doppler time is the time of closest approach, measured relative to an arbitrary time origin. Nadir is the point directly beneath the SAR i.e. the satellite projection on the earth. Swath is the width of the part of the Earth's surface that viewed by the satellite antenna. The range is direction of the platform to the target. Slant Range is the distance from the platform to the target. Ground range is the projection of Slant Range on the Earth's Surface. The direction in 90◦ to both slant range and ground range is

the azimuth direction. Near range is the edge of the swath closest to the nadir track .Far rang is the edge of the swath furthest to the nadir track [6]. the integration angle in the SAR geometry is presented in Fig. 3.3.

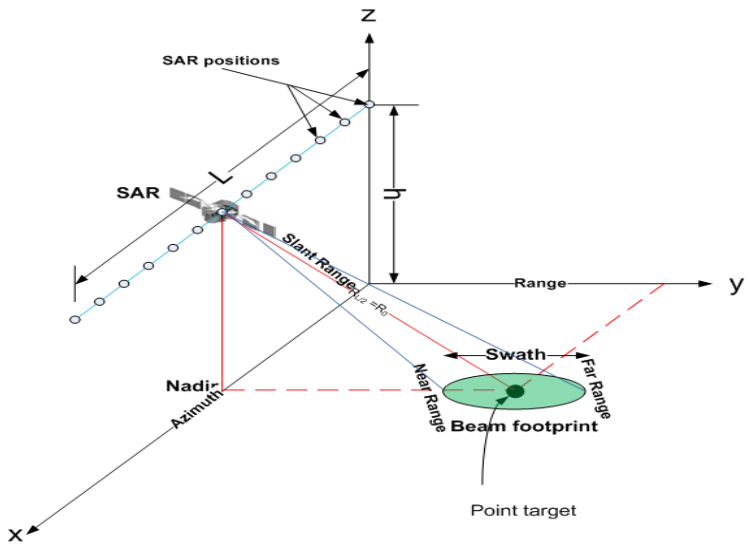

Fig. 3.2 Generic SAR imaging geometry.

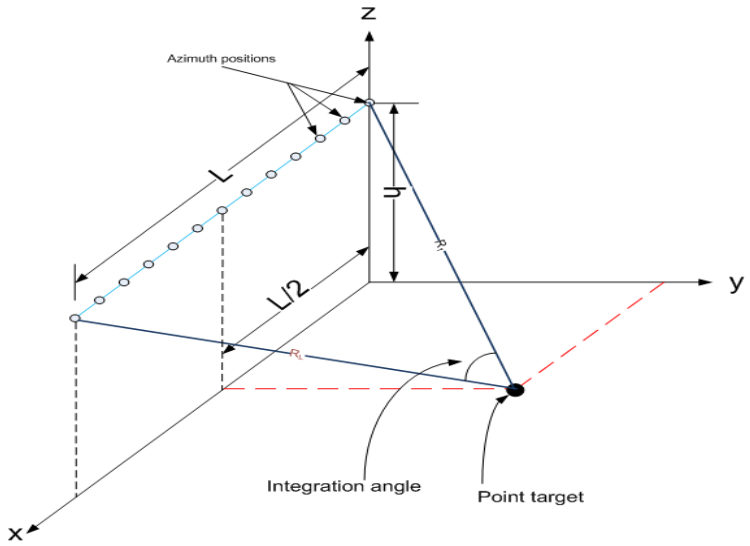

Fig. 3.3 Integration angle

3.4 SAR Resolution

The SAR resolution is defined as the smallest distance between two targets that allows the two targets still can be discerned. Since the SAR produce a two dimensional image, there are two resolutions, range resolution and azimuth resolution. The range resolution is determined by the transmitted pulse width (the length of the pulse in time), i.e. fine range resolution is obtained using a wide frequency bandwidth i.e. a narrow pulse in time domain. The azimuth resolution is perpendicular to range. It is defined by the sharpness of the beam (the lobe width) which is calculated by the wave length divided by the physical size of the antenna. Fine azimuth resolution is obtained using high frequency or a long antenna [6].

3.5 Frequency down Conversion

A frequency down conversion is a fundamental part in many communication systems such as satellite communication. Frequency down conversion allows the frequency band of interest to be moved down the spectrum so the sampling rate can be reduced and the processing on the signal of interest become more easily. In GPS case, the carrier frequency is $f1 = 1.57542\ GHz$ and the C/A code bandwidth is $2.046\ MHz$. The frequency down conversion allows selecting the $2.046\ MHz$ bandwidth and shifting its frequency down to base band and reducing the sampling rate. In fixed receiver bi-static SAR, the receiver is a dual channel receiver. The first channel is connected to an antenna pointed towards the satellite to obtain the direct signal. The second channel connected to an antenna pointed towards the target to receive the scattered signal. Both signals are down converted to an intermediate frequency (IF) and sampled with a suitable sampling rate [10]. This operation is depicted in Fig. 3.4.

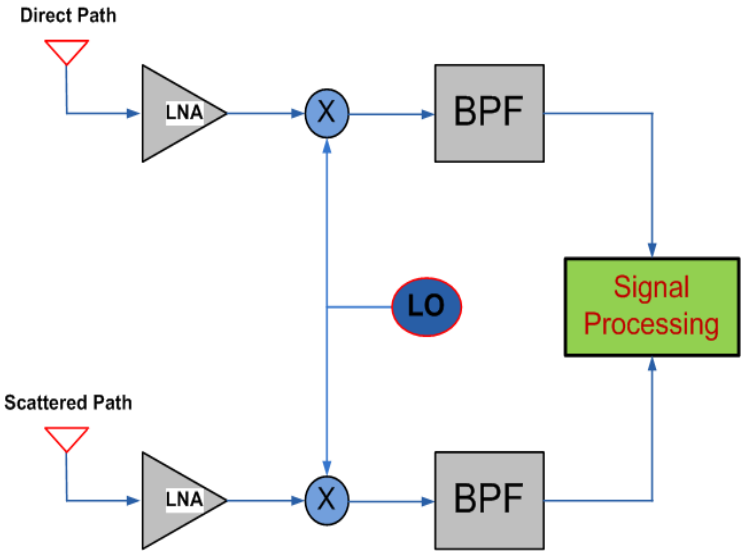

Fig. 3.4 BSAR dual channel receiver. The first channel receives the direct signal from the satellite. The second channel receives the scattered signal from the target. Both signals are down-converted to an intermediate frequency, then sampled at low sampling frequency.

The basic idea behind the dow- conversion operation is based on the following trigonometric identity

$$cos(A)cos(B) = \frac{1}{2}(cos(A+B) + cos(A-B))$$

And then by using a band-pass filter, it gives the required low frequency.

CHAPTER 4

SAR Image Forming Algorithms

SAR image forming algorithms can be organized into two main groups, frequency domain algorithms and time domain algorithms. This chapter gives a brief introduction to the two types and describes in more details the Global Back-Projection (GBP) algorithm [1] since it has been chosen as an image formation algorithm in this project.

4.1 Frequency-Domain Algorithms

The early SAR systems mostly use Fast Fourier Transform (FFT) based algorithms or frequency-domain algorithms due to their computational efficiency. They have a main drawback that they are valid only for a linear aperture (flight track) which is an assumption that is not applicable for an ultra-wideband system [11][12]. Some of the common frequency-domain algorithms are Range Doppler (RD) algorithm [13], Range Migration (RM) algorithm [14], Chirp Scaling (CS) Algorithm [15][16].

4.2 Time -Domain Algorithms

The time-domain algorithms are also known as back-projection algorithms. Time domain algorithms are used to solve the frequency-domain algorithms drawbacks in a cost of the computational efficiency. Some of the common time-domain algorithms are Global Back-projection (GBP) [11], Fast Back-projection (FBP) [17], and Fast Factorized Back-projection (FFBP) [18].

4.3 Comparative Features of Imaging Algorithms

This section describes the relative advantages and disadvantages for the algorithms in both domains.

FFT-based algorithms produce good image quality and try to reduce the processing load for non-wideband SAR while the image quality is not good in case of Ultra Wide Band (UWB) SAR. This is due to the long integration times needed by UWB SAR which require motion compensation for a good image quality. The FFT-based algorithms provide motion compensation, so they are not suitable for UWB SAR. The time-domain algorithms can provide the adequate motion compensation therefore they can work satisfactorily for UWB SAR systems [12][19].

Another drawback of FFT-based UWB algorithms is that, they require interpolation of data in frequency domain and this may lead to some errors that degrade the resulting image quality [17].

For the FFT-based algorithms the dimension of the data is related to the size of the image scene and this needs a large memory space since it normally processes a big data set [19].

Generally it can be said that the relative merits of time-domain algorithms over the frequency-domain algorithms are: wide bandwidth, unlimited scene size, perfect motion compensation, and ability to handle long integration angles while the relative drawback, they require heavy computational load. So the images can be produced with back-projection methods in the time domain or with FFT-based methods in the frequency domain and the choice is a trade-off between accuracy and computational load [19].

4.4 Global Back-projection

The Global Back-Projection (GBP) algorithm is the first time-domain algorithm which is a point-by-point reconstruction method, and it has been introduced with several advantages and it is considered as the root of all time-domain algorithms in the area of UWB SAR image scene construction. GBP is adapted to general aperture configuration, and compensating for range migration easily in the time domain, and it is characterized by the high resolution and low efficiency. Usually the evaluation of any new time-domain algorithm is performed by a comparison of the performance of GBP with the proposed algorithm [11][12].

The main steps in GBP are:

I. Compressing the range by the required method.
II. Dividing the scenes into a matter of cells, according to resolution and computational efficiency.
III. Calculating the transmitter-cells-receiver range by getting the first echo data.
IV. Projecting the scatter coefficients of each cell, according to the transmitter-cells-receiver range. Here, interpolation can be used. Linear interpolation, nearest neighbor interpolation, and cubic spline interpolation can be chosen as the interpolated functions.
V. Getting the next echo data and repeating step(III), until the last echo data are projected to the scenes.

In order to describe the global back projection in more details, consider a SAR raw data matrix generated from the sampled echoes from L SAR pulses. A row in the matrix corresponds to a particular pulse, in other words, to a platform position along the flight path; while a column corresponds to a particular range. The task for GBP is the integration for each resolution cell in the output image, the instantaneous response that a target in that particular cell would have. This is shown in Fig. 4.1. , where the image of size MxN pixels is created. Every pixel of the MxN pixels in the resulting image is produced by L additions where N is the azimuth size, M is range size, and L SAR pulses correspond to the full radar integration length, or aperture. Thus the computational complexity is proportional to *LxMxN* [11][12]. Using other back-projection method will reduce the computational complexity.

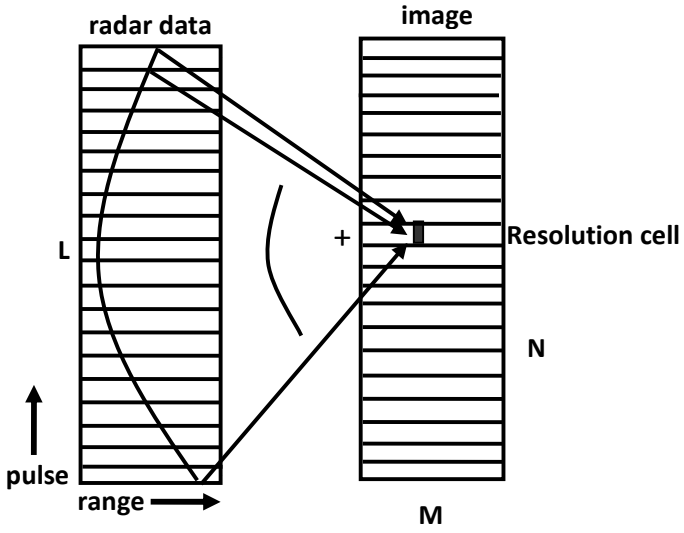

Fig. 4.1 Simplified illustration of global back-projection [1]

CHAPTER 5

Simulation Models and Results

The goal of this thesis work is to investigate the fixed receiver Bi-Static SAR image formation using C/A code and GBP. To perform this task, a MATLAB simulation was done. The performance of the bi-static SAR is compared with the monostatic SAR. Also, different receiver locations are taken into account. The following sections describe the simulation models and the results obtained from the simulation.

5.1 Monostatic Image Processing and Formation

This part describes the monostatic SAR image formation model. It presents the system geometry and clarifies the location of the point target, the platform movement, the signals representation, and the relevant parameters.

5.1.1 System Geometry

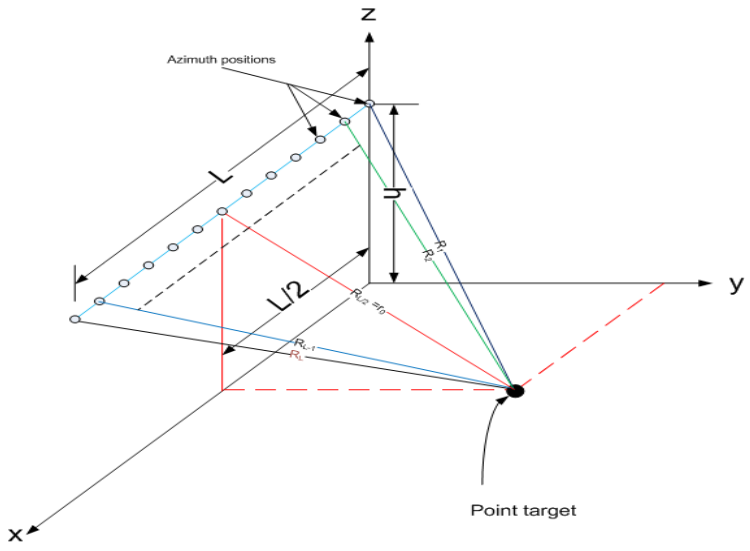

Fig. 5.1. Monostatic SAR imaging geometry. At each azimuth position, the pulse propagates between the antenna and the target, and back again after being back-scattered by the target.

Fig. 5.1 presents the monostatic SAR system geometry used in this work; it presents a point target which is located at (x_0, y_0, z_0) and SAR system. The platform flying is assumed to be in the same direction as the $X-$axis with constant speed $(128\ m/s)$ at constant altitude $(2000\ m)$ i.e. the flying path is assumed to be a straight line. The point target is located on the ground, in the middle of the aperture length $(L/2)$ and $(1500m)$ away from the flying trajectory (ground range) i.e. at the location $(x_0, y_0, z_0) = (1035.5m, 1500m, 0m)$. Table 5.1 shows the main parameters related to this model.

Table 5.1 Monostatic SAR Model Parameters

Parameter	Value
Altitude \ h	2000 [m]
Ground range	1500[m]
Integration angle	45[degrees]
Platform velocity\ v	128[m/s]
Pulse repletion frequency \PRF	100 [Hz]
Full aperture length	2070[m]
Number of aperture positions	1618

5.1.2 Signals Representations

In the case under study, it is assumed that the system transmits a pulse and waits in the same aperture position to receive the scatter from the target, then moves to the next position, transmits a new pulse and waits to receive the scatter, and so on.

The transmitted signal is the C/A code modulated with QPSK modulation technique, and the received signal is a delayed version of the transmitted signal; this operation is repeated for every aperture position. The delay for each position is related to the duple of the slant range of that position and it is given by:

$$\tau(n) = \frac{2 * R(n)}{c} \tag{5.1}$$

where $\tau(n)$ is time delay of the received signal at the position n, $R(n)$ is the distance between the target and the transmitter at the position n, and c is the speed of light. $R(n)$ is calculated using the following formula:

$$R(n) = \sqrt{(Xt(n) - Xp)^2 + (Yt(n) - Yp)^2 + (Zt(n) - Zp)^2} \quad (5.2)$$

where $Xt(n)$, $Yt(n)$ and $Zt(n)$ are the platform coordinates at n and Xp, Yp and Zp are the target coordinates.

The channel effect (path loss, fading, attenuation…etc) has been ignored only the phase shift (due to the delay) is considered. Table 5.2 presents the frequencies and times considered during the simulation. Note the carrier frequency is chosen to be 10.23MHz and not 1575.42MHz. This selection is made in order to decrease the computational cost.

Table 5.2 Frequencies And Times

Parameter	Value
C/A code frequency \ fb	1.023[MHz]
C/A code bit duration \Tb	0.9975[µs]
C/A code length \ Tc	1[ms]
Light speed \ c	3x10^8 [m/s]
Carrier frequency \fc	10.23 [MHz]
Sampling frequency \Fs	40.92 [MHz]
Sampling time \Ts	0.024438[µs]

5.1.3 Data Acquisition and Processing

At each azimuth position, the received signal is compressed by correlating the received signal with a reference signal at the receiver; the result is stored as a row in a matrix. This operation is repeated for all azimuth positions, then, the SAR raw data matrix (two dimensional) is generated. A row in the matrix corresponds to a particular pulse while a column corresponds to a particular target range.

After data acquisition and generating the SAR raw data, the global back-projection algorithm is applied for this data in order to generate the final SAR image for a selected area of size (400 pixels x 400 pixels) considering that the point target in the middle of this area.

5.1.4 Results and Analysis

Following the above descriptions, the system was simulated in Matlab. The following paragraph discusses the obtained results.

As previously mentioned, in the algorithm implementation stage, the received signals had been compressed using a cross-correlation method which correlates the received signals with a reference signal generated in the receiver, and this operation is performed at every aperture position. Fig. 5.2 shows the last received signal after compression.

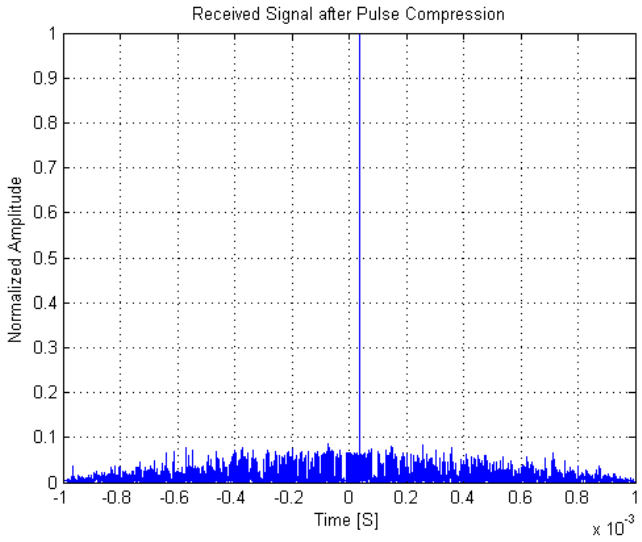

Fig. 5.2 Received signal after compression. The received signal is compressed using the correlation method. The position of maximum value is related to the double of the slant range.

All of the compressed received signals were stored in a matrix form in order to make it suitable for the data processing stage. Fig. 5.3 presents the received signal in two dimensional signal memory. Fig. 5.4 is a zoomed version of Fig. 5.3. From Fig. 5.3 and Fig. 5.4, it can be seen that the received signal strength gets its maximum value at the center of the aperture and it gets reduced when moving away from the center. This Phenomenon can be interpreted from the auto-correlation properties since it is known that the maximum auto-correlation value $R(\tau)$ for any signal $S(t)$ is at $\tau = 0$ i.e. $\max |R(\tau)| = R(0) \Rightarrow \tau = 0$; while the maximum auto-correlation value for any signal $S(t)$ and a delayed version of that signal $S(t - t_1)$ at $\tau = t_1$. i.e. $max\ |R(\tau - t_1)| = R(0) \Rightarrow \tau = t_1$; this case correspond to the monostatic case, and the time delay for any received signal is related to the double of the slant range for the corresponding aperture position. The minimum slant range is at the center of the aperture and it is increased when moving far away from the centre. This interprets the hyperbolic curved line of the SAR raw data in Fig. 5.3 and Fig. 5.4.

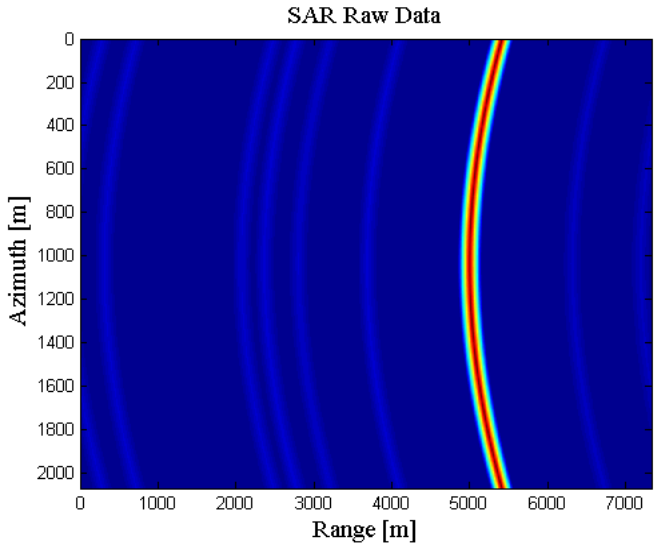

Fig. 5.3 Received SAR data in two-dimensional signal memory. A row in the matrix corresponds to a particular pulse while a column corresponds to a particular target range. The position of maximum value is related to the double of the slant range of the corresponding azimuth position.

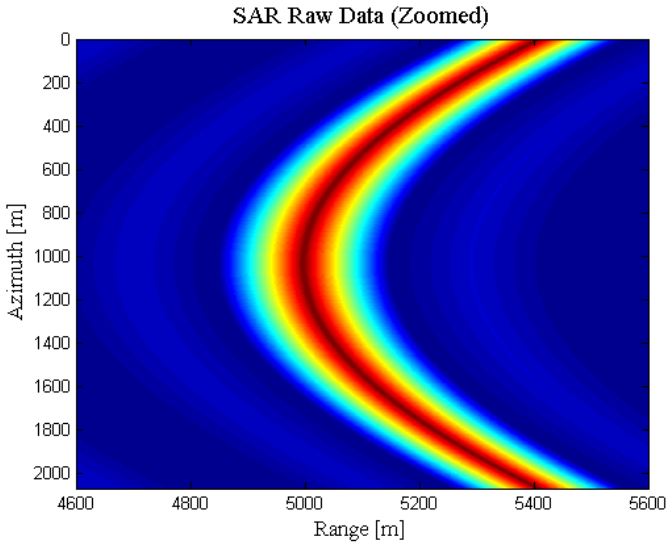

Fig. 5.4 A zoomed received SAR data in two-dimensional signal memory. This is a zoomed version of Fig. 5.3.

The GBP was applied for the SAR raw data matrix in order to generate the final SAR image of an area of 400 pixels x400 pixels, the result is shown in Fig. 5.5; this is the main figure in the whole story since it represents the final SAR image corresponding to the point target. The resolution is the major factor used in this work in order to compare the performance of different configurations, as previously mentioned there are two resolutions, azimuth resolution and range resolution. To measure the resolution the contour plots of the final SAR image is generated and presented in Fig. 5.6 for the levels $[0dB - 3dB - 6dB - 12dB - 15dB - 18dB - 24dB]$, the resolution is determined by the $-3dB\ level$ and the lower levels represent the sidelobes. Fig. 5.7 represents a zoomed version of Fig. 5.6 in order to clearly show the $-3dB\ level$. It can be shown from Fig. 5.7 that the resolution in the range direction is $\Delta r = 100m$ while in the azimuth direction is $\Delta a = 12m$. The azimuth resolution values are related to the center frequency which is not $1575.42\ MHz$ but chosen to $10.23\ MHz$ in this simulation.

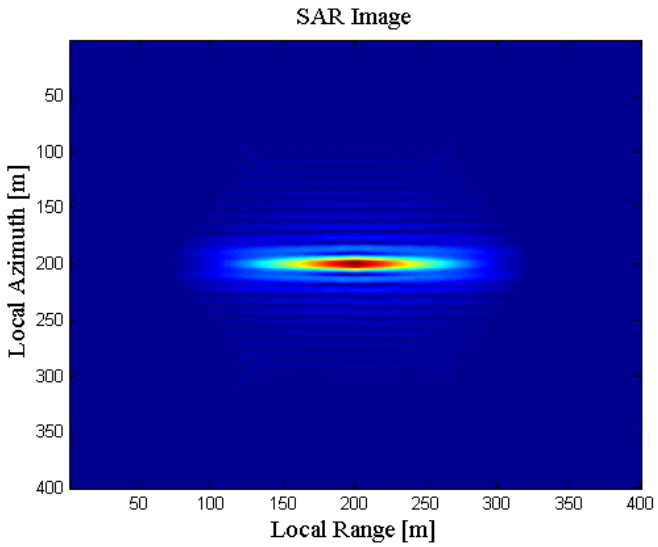

Fig. 5.5 Final monostatic SAR image of the point target. The final SAR image of an area of 400 pixels x400 pixels is generated by applying the GBP for the SAR raw data of Fig. 5.3.

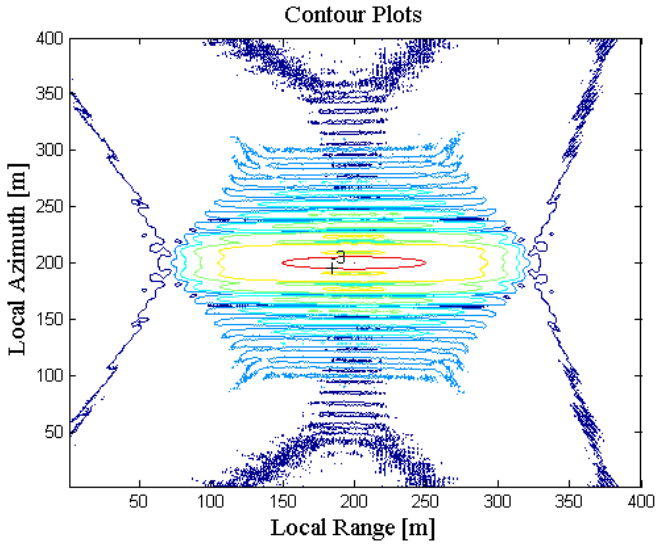

Fig. 5.6 The contour plots of the point target. The contour pots is generated for the levels [0 dB -3 dB -6 dB -12 dB -15 dB -18 dB -24 dB]

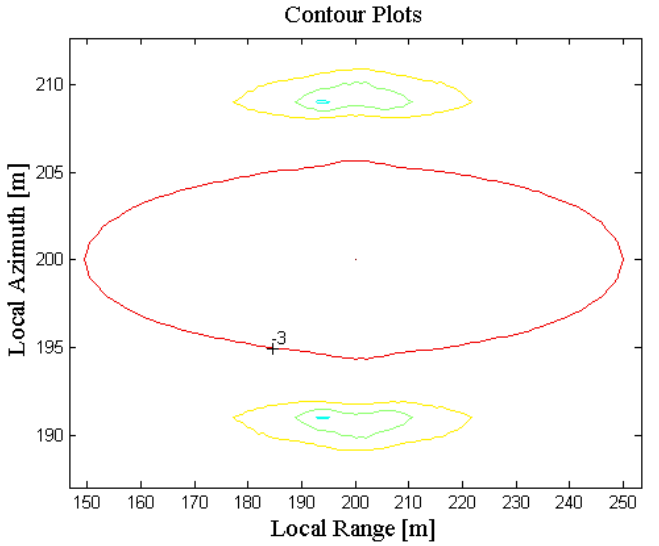

Fig. 5.7 A zoomed contour plots. To measure the resolution, the -3dB contour plot is zoomed. The resolution in the range direction is $\Delta r = 100m$ while in the azimuth direction is $\Delta a = 12m$.

An alternative method to measure the resolution, is to extract two vectors in the middle of the SAR image in azimuth and range directions, the resolution is the distance between the two points at which the intensity is one half of the peak intensity. Fig. 5.8 and Fig. 5.9 present the two vectors extracted from the middle SAR image in the range

and azimuth directions respectively. Fig. 5.8. shows the resolution in the range direction is $\Delta r = 100m$ also it can be seen that there are no sidelobes in range and this is due to the code characteristics and the selected area is small. Fig. 5.9 shows the resolution in azimuth direction is $\Delta a = 12m$. The SAR image spectrum in frequency domain corresponds to this point target is produced and presented in Fig. 5.10.

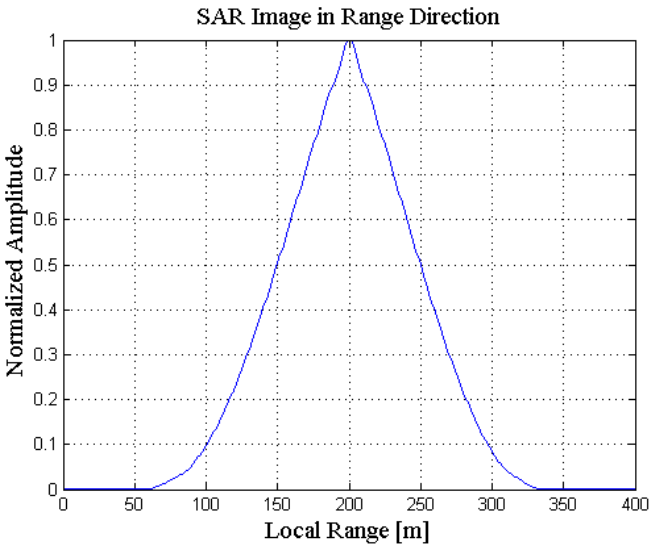

Fig. 5.8 Middle SAR image vector in range direction. The resolution in the range direction is $\Delta \mathbf{r} = \mathbf{100m}$ which is the distance between the two points at which the intensity is one half of the peak intensity.

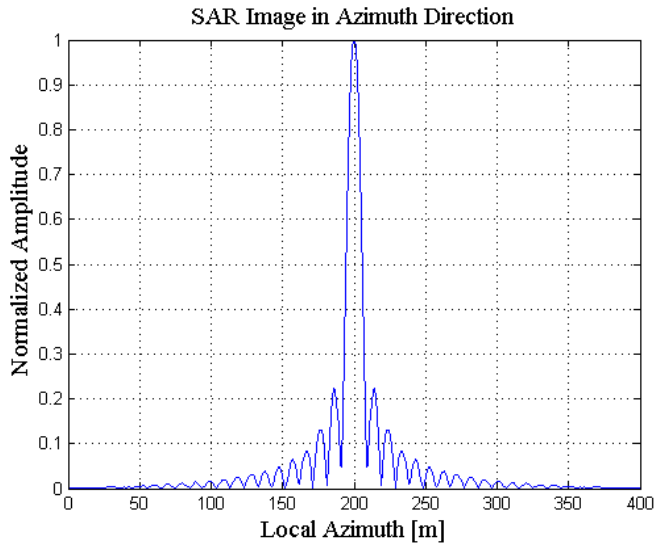

Fig. 5.9 Middle SAR image Vector in Azimuth Direction. The resolution in azimuth direction is $\Delta a = 12\mathrm{m}$ which is the distance between the two points at which the intensity is one half of the peak intensity.

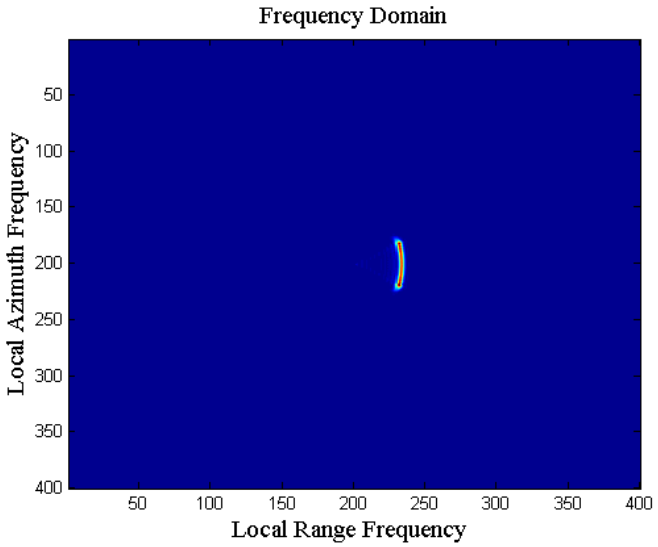

Fig. 5.10 Monostatic SAR image in 2D- frequency domain

The above discussions presented the results for monostatic case which will be used as a basis of comparison to the bi-static configuration. As previously mentioned, the difference between the two configurations is the location of the receiver only. The bi-static case is presented in the following paragraphs.

5.2 Bistatic Image Processing and Formation

This part describes the bi-static SAR image formation model. In this case, it is assumed that, the receiver is located on a tower somewhere above the ground looking down to the illuminated scene. Normally in a bistatic setup the bistatic angle is small as in [20], has flight passes in parallel as in [21] or has the flight track and the receiver on the same side of the target. This is not the case in our study.

5.2.1 Case Study No (1)

This case gives the best resolution. It will be investigated in more details and the results will be compared to the monostatic case performance.

5.2.1.1 System Geometry

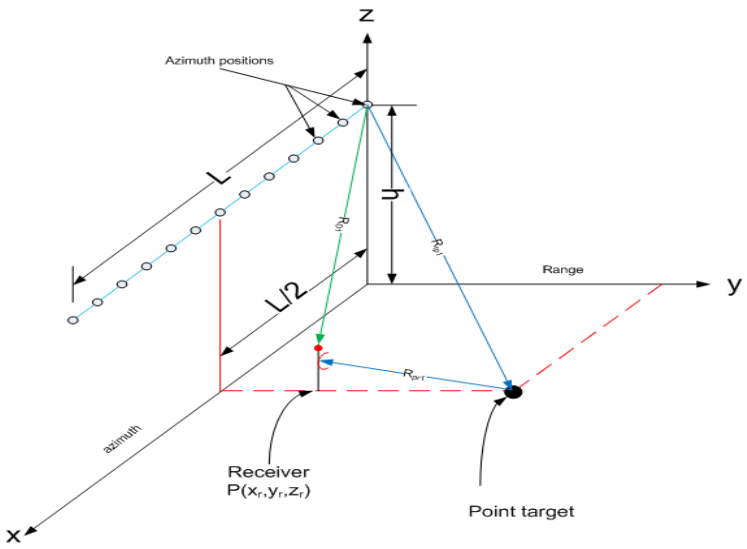

Fig. 5.11 Fixed-receiver bistatic SAR imaging geometry. At every azimuth position the receiver receives tow signals, the first one is the direct signal from the satellite and the second one is the scatter from the target.

Fig. 5.11 presents the bi-Static SAR model, it can be seen that the only difference compared to monostatic is the location of the receiver. The same parameters summarized in Table 5.1 and Table 5.2 will be used, in addition, a new parameters that define the location of the receiver is added and it is shown in Table 5.3. The location of the receiver, in comparison to the target and the transmitter, is important, for example it affects the

resolution. In this study, different locations have been considered and it will be clarified later in this chapter.

Table 5.3 The receiver location

	X-axis [m]	Y-axis [m]	Z-axis [m]
Point target	1035.5	1500	0
Reciever	1035.5	500	100

5.2.1.2 Signals Representations

Similar to the monostatic case, at each azimuth position, the transmitted signal is the C/A code modulated with QPSK modulation technique, and then the received signal is a delayed version of the transmitted signal. However, in this case, the receiver receives two signals, the first one is the direct signal from the transmitter and the second one is the scatter from the target. The delay for each signal is related to the distance that is travelled by that signal. Hence, there exist two delays that should be calculated at each azimuth position.

The delay for the direct signal is given by

$$t_1(n) = \frac{R_1(n)}{c} \tag{5.3}$$

where $t_1(n)$ is time delay of position n, $R_1(n)$ is the distance between the transmitter and the receiver, and c is the speed of light. $R_1(n)$ is calculated using the following formula

$$R_1(n) = \sqrt{(X_t(n) - X_r)^2 + (Y_t(n) - Y_r)^2 + (Z_t(n) - Z_r)^2} \tag{5.4}$$

where$X_t(n)$, $Y_t(n)$ and $Z_t(n)$ are the SAR transmitter coordinates at position n, and X_r, Y_r and Z_r are the receiver coordinates.

The delay for the signal reflected from the target is given by

$$t_2(n) = \frac{R_2(n)}{c} \tag{5.5}$$

where $t_2(n)$ is the time delay correspond to position n, $R_2(n)$ is the distance from the transmitter to the target and then to the receiver, and c is the speed of light. $R_2(n)$ is a summation of two distances

$$R_2(n) = R_3(n) + R_4 \tag{5.6}$$

$R_3(n)$ is the distance from the transmitter to the target and is given by

$$R_3(n) = \sqrt{(X_t(n) - X_p)^2 + (Y_t(n) - Y_p)^2 + (Z_t(n) - Z_p)^2} \tag{5.7}$$

where $X_t(n)$, $Y_t(n)$, and $Z_t(n)$ are the SAR coordinates at the position n, and X_p, Y_p, and Z_p are the target coordinates.

R_4 is the fixed distance from the receiver to the target and is given by

$$R_4 = \sqrt{(X_r - X_p)^2 + (Y_r - Y_p)^2 + (Z_r - Z_p)^2} \tag{5.8}$$

where X_r, Y_r, and Z_r are the SAR receiver coordinates, and X_p, Y_p, and Z_p are the target coordinates.

5.2.1.3 Data Acquisition and Processing

At each azimuth position, the received signal is compressed by correlating the two received signals; the result is stored as a row in a matrix. After repeating this operation for all azimuth positions, the SAR raw data matrix (two dimensional) is generated. Each row in the matrix corresponds to a particular pulse while each column corresponds to a particular target range.

After data acquisition and generating the SAR raw data, similar to the monostatic case, but taking into account that two time delays will be calculated, the global back-projection algorithm is applied for this data in order to generate the final SAR image for a selected area of size (400 pixels x 400 pixels) considering that the point target in the middle of this area.

5.2.1.4 Results and Analysis

Following the above descriptions, the systems were simulated in Matlab. The simulation results for the case presented in Fig. 5.11 .i.e. the receiver is located in the position $pr\ (x, y, z)\ = pr(1035.5,500,100)$ are discussed below.

Fig. 5.12 shows the last received signal after compression while Fig. 5.13 and Fig. 5.14 present the received signals in two dimensional memory and a zoomed version of this signal respectively. In this case the cross-correlation is performed for a two delayed signals $S(t - t_1)$ and $S(t - t_2)$ of the transmitted signal $S(t)$. Here the maximum cross-correlation value at the difference i.e. $\tau = t_2 - t_1$. In other words, $max\ |R(\tau - t_1 + t_2)\ | = R(0) \Rightarrow \tau = t_2 - t_1$; This interprets the results obtained. Comparing Fig. 5.12. for bi-static with Fig. 5.2 for monostatic, it can be seen that the maximum value of Fig. 5.12 is more close to zero and this is because it depends on the time difference $(\tau = t_2 - t_1)$ which is a small value compared with the value $(\tau = t_1)$ in the monostatic case. This time difference controls the shape of the raw data matrix so various shapes can be obtained depending on the location of the receiver, not like the monostatic case since in the monostatic case there is only the hyperbolic curved line of the SAR raw data.

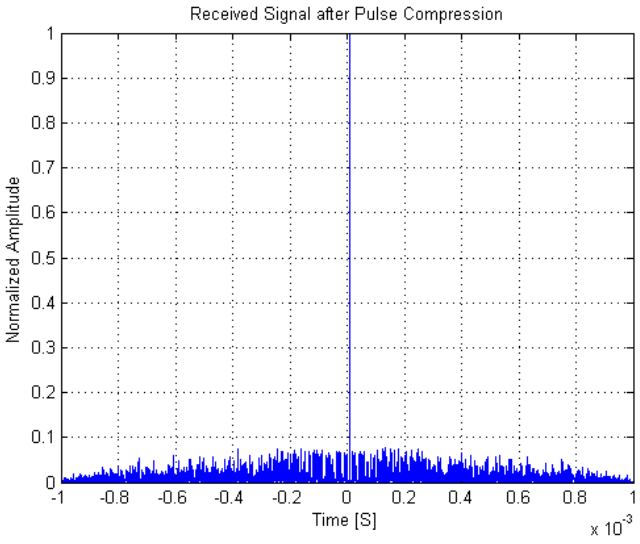

Fig. 5.12 Received signal after compression. The compressed pulse is generated by correlating the two received signals.

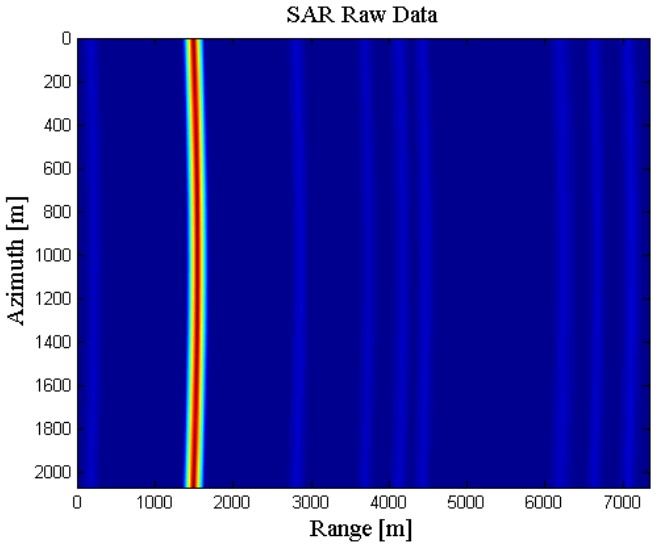

Fig. 5.13 Received SAR data in two-dimensional signal memory. A row in the matrix corresponds to a particular pulse while a column corresponds to a particular target range. The position of maximum value is related to the difference in the time delay of the two received signals at the corresponding azimuth position.

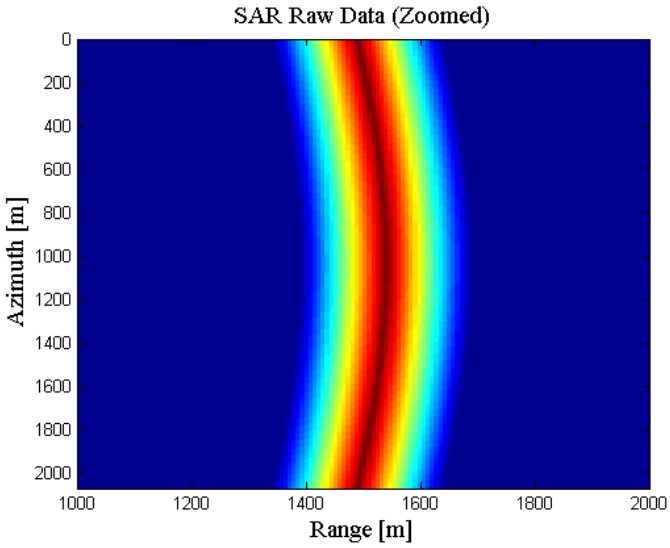

Fig. 5.14 A zoomed received SAR data in two-dimensional signal memory. This is a zoomed version of Fig. 5.13.

The GBP is applied for the SAR raw data matrix in order to generate the final SAR image of an area of $400\,pixels\,x\,400\,pixels$ and the result is shown in Fig. 5.15. As previously mentioned, the resolution is the most important factor of comparison considered in this work. The same procedures as in the monostatic case will be used here.

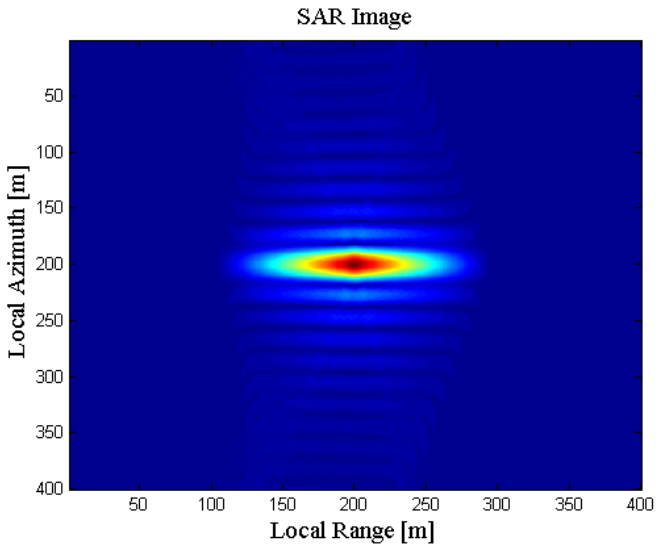

Fig. 5.15 Final bistatic SAR image of the point target. The final SAR image of an area of 400 pixels x400 pixels is generated by applying the GBP for the SAR raw data of Fig. 5.13.

The contour plots of the final SAR image is generated and presented in Fig. 5.16 for the levels $[0dB - 3dB - 6dB - 12dB - 15dB - 18dB - 24dB]$, as usual, the resolution is determined by the $-3dB\ level$ and the lower levels represent the side lobes. Fig. 5.17 represents a zoomed version of Fig. 5.16 in order to clearly show the $-3dB\ level$. It can be shown from Fig. 5.17 that the resolution in the range direction is $\Delta r = 92m$ while in the azimuth direction is $\Delta a = 22m$.

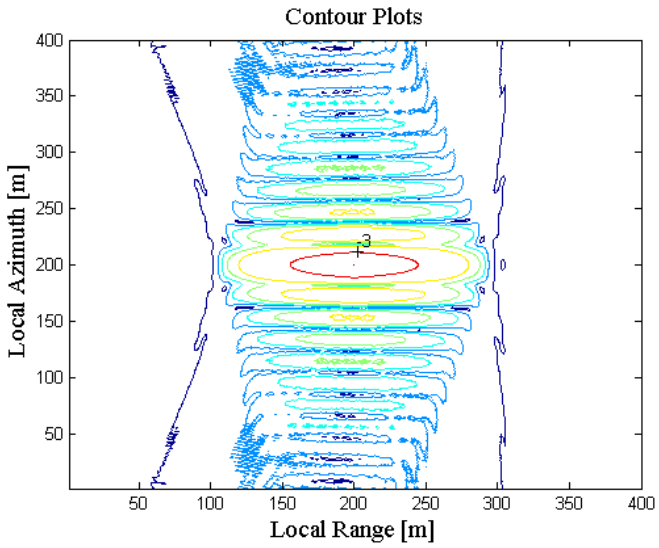

Fig. 5.16 The contour plots of the point target. The contour pots is generated for the levels [0 dB -3 dB -6 dB -12 dB -15 dB -18 dB -24 dB]

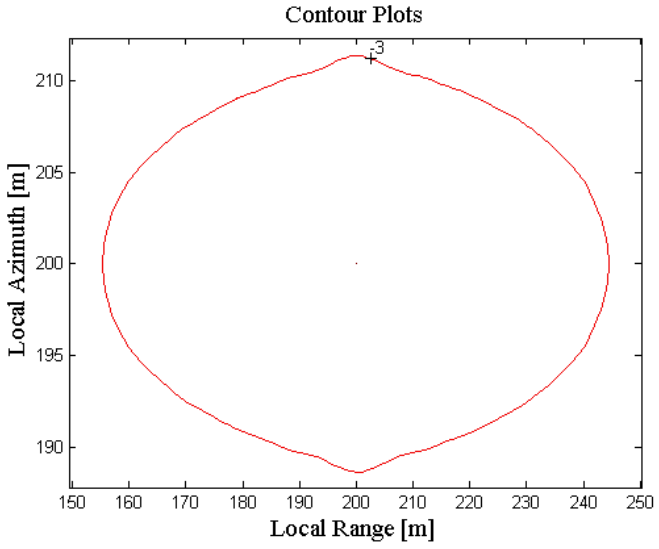

Fig. 5.17 A zoomed contour plots. To measure the resolution, the -3dB contour plot is zoomed. The resolution in the range direction is $\Delta r = 94m$ while in the azimuth direction is $\Delta a = 22m$.

Also the resolution can be measured using the alternative method. Fig. 5.18 and Fig. 5.19 present the two vectors extracted from the middle SAR image in the range and the azimuth directions respectively. Fig. 5.18 shows the resolution in the range direction is $\Delta r = 92m$, also it can be seen that there are no sidelobes and this due to the code

characteristics and the small selected area. Fig. 5.19 shows that, the resolution in the azimuth direction is $\Delta a = 22m$. The SAR image spectrum in frequency domain corresponds to this point target is produced and presented in Fig. 5.20.

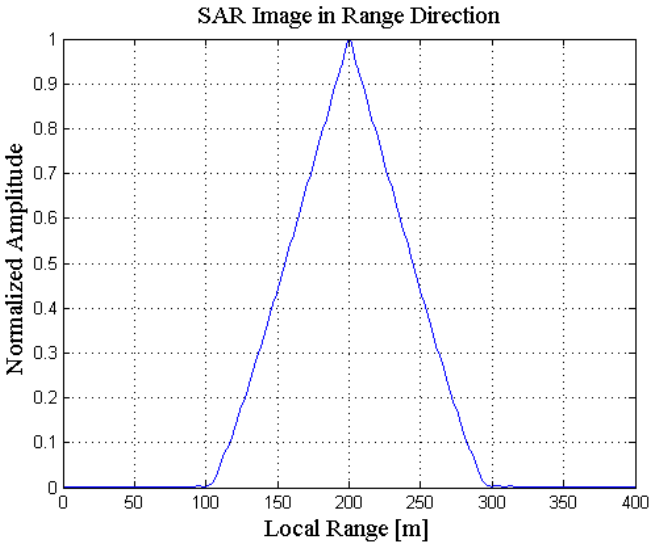

Fig. 5.18 Middle SAR image vector in range direction. The resolution in the range direction is $\Delta \mathrm{r} = 94\mathrm{m}$ which is the distance between the two points at which the intensity is one half of the peak intensity.

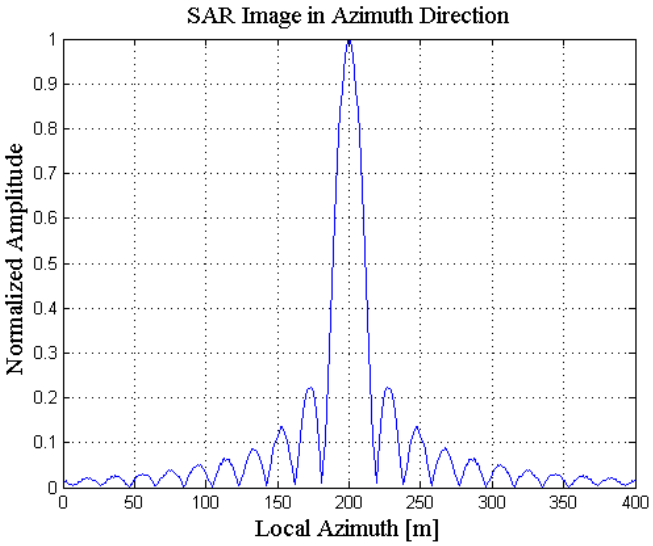

Fig. 5.19 Middle SAR image Vector in Azimuth Direction. The resolution in azimuth direction is $\Delta \mathrm{a} = 22\mathrm{m}$ which is the distance between the two points at which the intensity is one half of the peak intensity.

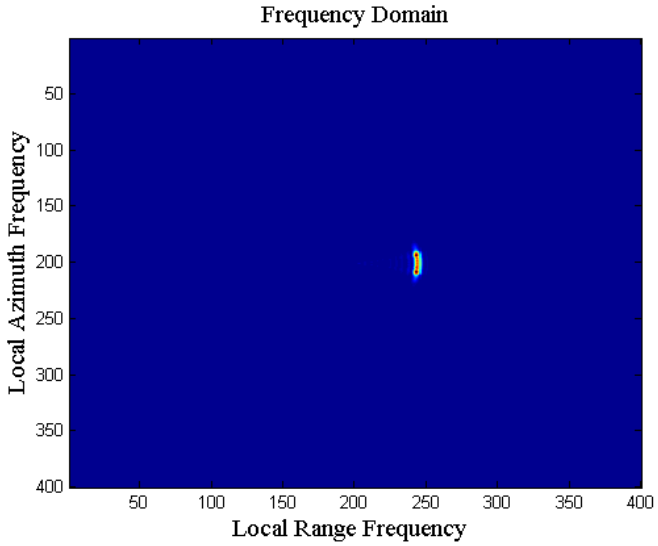

Fig. 5.20 Bistatic SAR image in 2D- frequency domain

Based on the obtained results, the monostatic configuration outperforms the bistatic configuration in azimuth direction; in bistatic configuration, the azimuth resolution is almost twice that of the monostatic case. Also, for this specific configuration, the bistatic configuration outperforms the monostatic configuration in range direction. The difference in range resolution, as it can be seen from Table 5.4, is not that much, so it can be said that they have the same performance in range direction. Table 5.4 summarizes the resolution obtained from the results of the two configurations.

Table 5.4 The performance of the monostatic SAR and the bistatic SAR.

Configuration	Range resolution [m]	Azimuth resolution [m]
Monostatic	100	12
Bi-static	94	22

The range resolution strongly depends on the receiver location in comparison to the transmitter and target locations. To prove this, various receiver locations have been considered, the results are discussed in the following sections.

The following sections discusse three other study cases for different receiver locations to show the effect of the position on the resolution.

5.2.2 Case Study No (2)

In this case, the receiver location coordinates are given in Table 5.5 and the system geometry is presented if Fig. 5.21.

Table 5.5 Receiver location for the case study no (2)

	X-axis [m]	Y-axis [m]	Z-axis [m]
Point target	1035.5	1500	0
Reciever	1035.5	2000	100

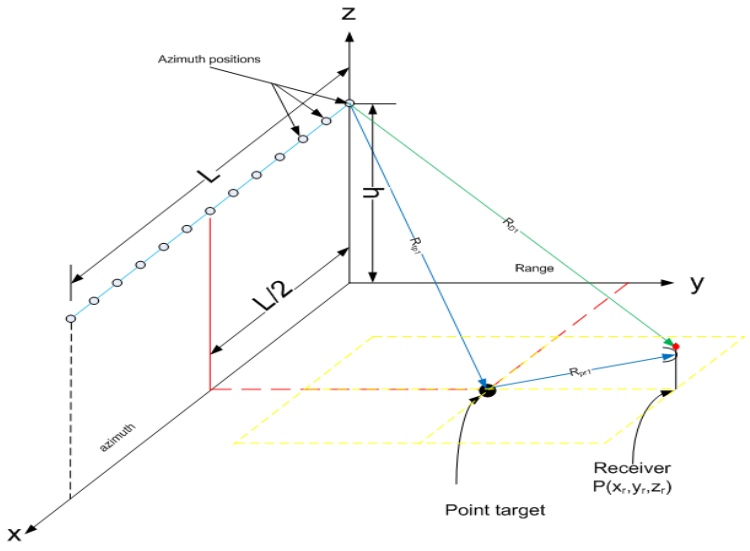

Fig. 5.21 Fixed-receiver bistatic SAR imaging geometry (case study no (2)). The target between the transmitter and the fixed receiver.

The results for case study are presented in Fig. 5.22. It depicts four figures. Fig. 5.22 (a) shows the received signals in a two dimensional memory, it can be seen that the signal strength is almost the same for all azimuth positions. Fig. 5.22 (b) depicts the resulting final SAR image for the area of (400 pixels x 400 pixels). Fig. 5.22 (c) presents the contour plots of the final SAR image, it shows the levels $[0\text{dB} - 3\text{dB} - 6\text{dB} - 12\text{dB} - 15\text{dB} - 18\text{dB} - 24\text{dB}]$, as before, the resolution is determined by the -3dB level and the lower levels represent the side lobes. Fig. 5.22 (d) represents the SAR image spectrum in frequency domain corresponds to the point target.

In order to determine the resolution, a zoomed version of Fig. 5.22 (c) is shown in Fig. 5.23. It clearly shows the $-3dB\ level$. It can be shown that the resolution in the range direction is $\Delta r = 340m$ while in the azimuth direction is $\Delta a = 22m$.

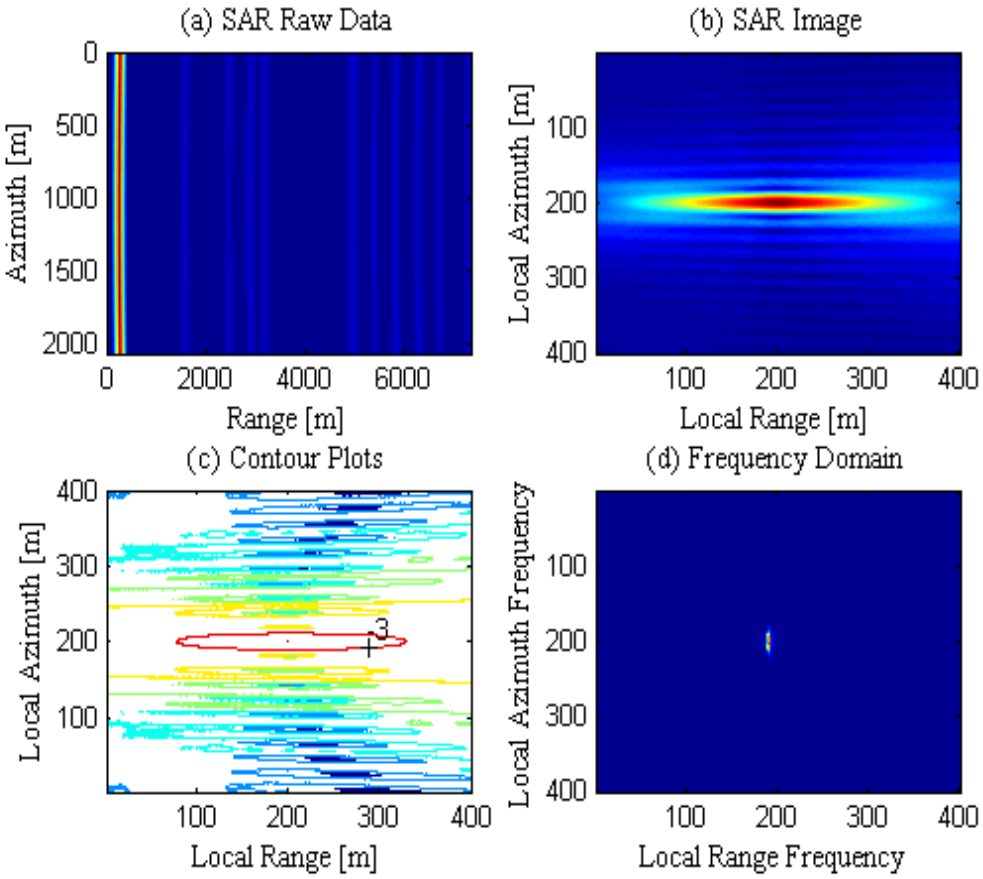

Fig. 5.22 Results of case study no (2). (a) Received SAR data in two-dimensional signal memory. (b) Final bistatic SAR image of the point target. (c) The contour plots of the point target. The contour pots is generated for the levels [0 dB -3 dB -6 dB -12 dB -15 dB -18 dB -24 dB]. (d) Bistatic SAR image in 2D- frequency domain

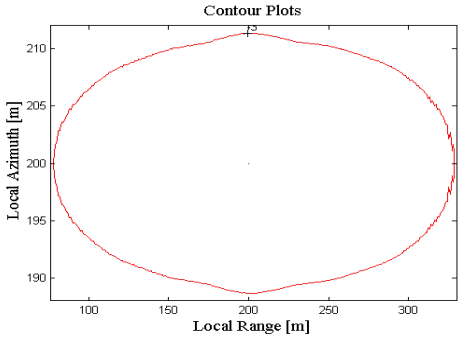

Fig. 5.23 A zoomed contour plots. To measure the resolution, the -3dB contour plot is zoomed. The resolution in the range direction is $\Delta r = 340m$ while in the azimuth direction is $\Delta a = 22m$.

5.2.3 Case Study No (3)

In this case, the receiver location coordinates are given in Table 5.6 and the system geometry is presented if Fig. 5.24.

Table 5.6 Receiver location for the case study no (3)

	X-axis [m]	Y-axis [m]	Z-axis [m]
Point target	1035.5	1500	0
Reciever	535.5	500	100

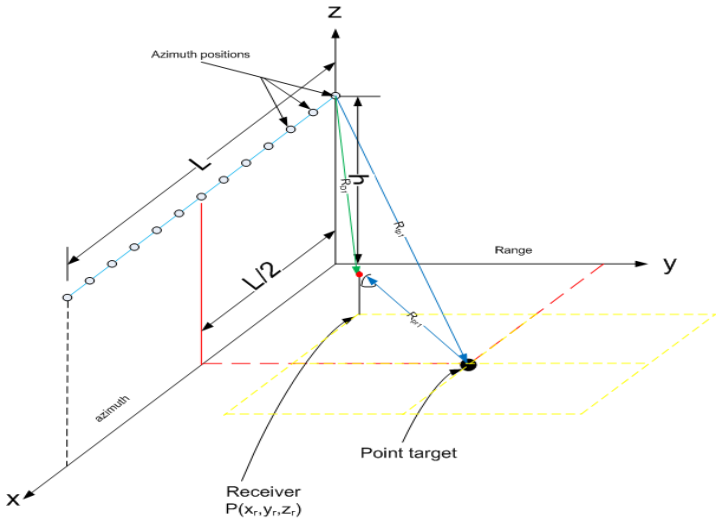

Fig. 5.24 Fixed-receiver bistatic SAR imaging geometry (case study no (3)). The fixed receiver is located between the transmitter and the target.

Similar to the case study no (2) results, the results for this case study are presented in Fig. 5.25. Fig. 5.25 (a) shows the received signals in a two dimensional memory, it can be seen that the SAR raw data shape is different compared to the previous bi-static cases (Fig. 5.13 and Fig. 5.22 (a)). Fig. 5.25 (b) depicts the resulting final SAR image for the area of $(400\,pixels\,x\;400\,pixels)$. Fig. 5.25 (c) presents the contour plots of the final SAR image, it shows the levels $[0dB - 3dB - 6dB - 12dB - 15dB - 18dB - 24dB\,]$. In this case also, the resolution is determined by the $-3dB\;level$ and the lower levels represent the side lobes. Fig. 5.25 (d) represents the SAR image spectrum in frequency domain corresponds to the point target.

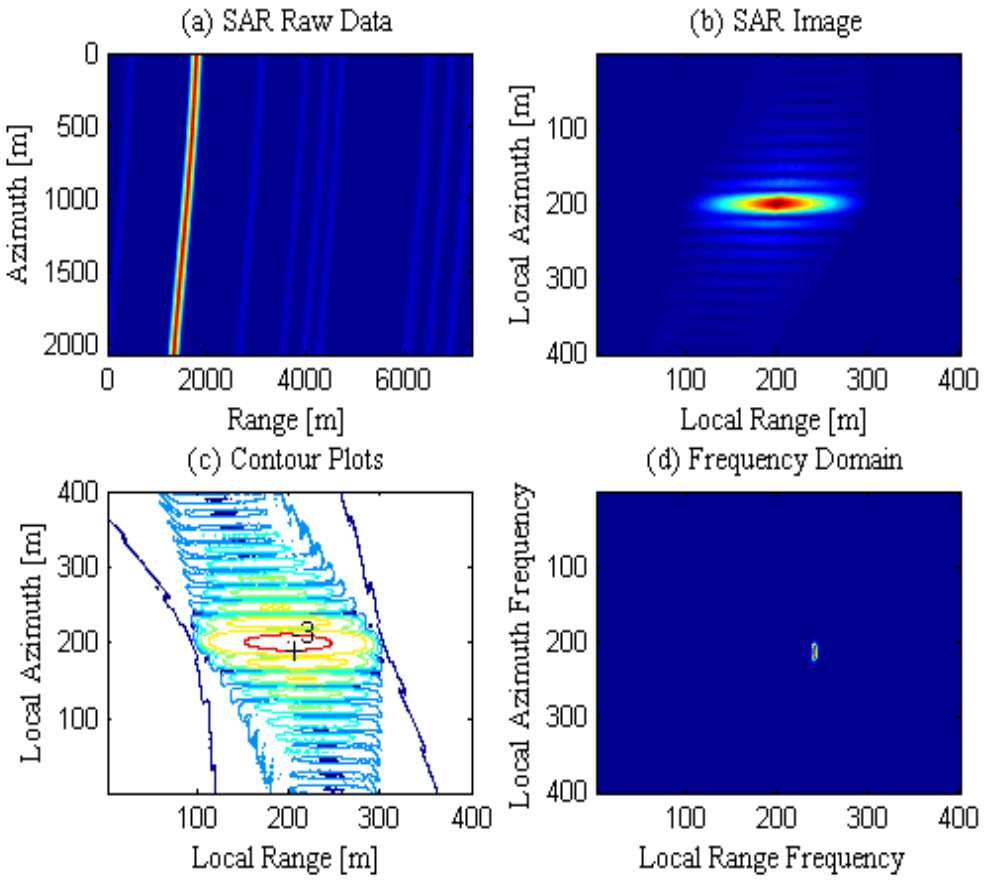

Fig. 5.25 Results of case study no (3). (a) Received SAR data in two-dimensional signal memory. (b) Final bistatic SAR image of the point target. (c) The contour plots of the point target. The contour pots is generated for the levels [0 dB -3 dB -6 dB -12 dB -15 dB -18 dB -24 dB]. (d) Bistatic SAR image in 2D- frequency domain

In order to determine the resolution, a zoomed version of Fig. 5.25 (c) is shown in Fig. 5.26. It clearly shows the $-3dB\ level$. It can be shown that the resolution in the range direction is $\Delta r = 96m$ while in the azimuth direction is $\Delta a = 22m$.

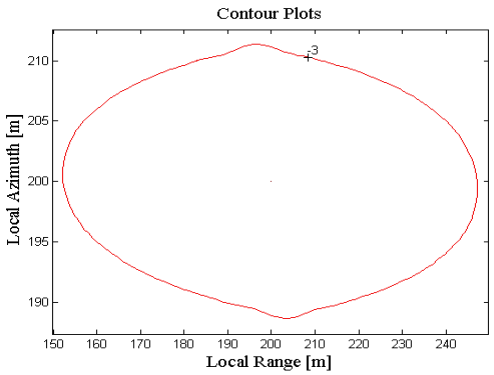

Fig. 5.26 A zoomed contour plots. To measure the resolution, the -3dB contour plot is zoomed. The resolution in the range direction is $\Delta r = 96m$ while in the azimuth direction is $\Delta a = 22m$.

5.2.4 Case Study No (4)

In this case, the receiver location coordinates are given in Table 5.7 and the system geometry is presented in Fig. 5.27.

Table 5.7 Receiver location for the case study no (4)

	X-axis [m]	Y-axis [m]	Z-axis [m]
Point target	1035.5	1500	0
Reciever	1535.5	500	100

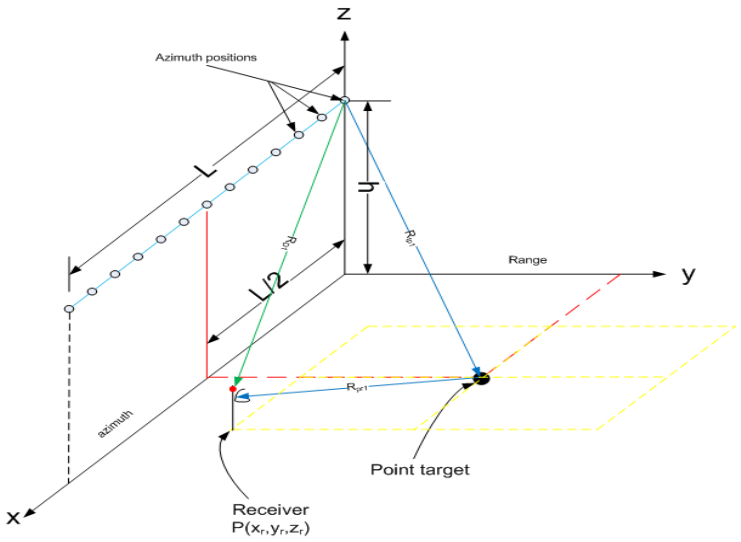

Fig. 5.27 Fixed-receiver bistatic SAR imaging geometry (case study no (4)). The fixed receiver is located between the transmitter and the target.

Similar to previous cases, the results for this case study are presented in Fig. 5.28. Fig. 5.28 (a) shows the received signals in a two dimensional memory, also it can be seen that the SAR raw data shape is different compared to the previous bi-static cases. The Fig. 5.28 (b) presents the resulting final SAR image for the area of $(400\ pixels\ x\ 400\ pixels)$. Fig. 5.28 (c) presents the contour plots of the final SAR image, it shows the levels $[0dB - 3dB - 6dB - 12dB - 15dB - 18dB - 24dB\ ]$. As before, the resolution is determined by the $-3dB\ level$ and the lower levels represent the side lobes. Fig. 5.28(d) represents the SAR image spectrum in frequency domain corresponds to the point target.

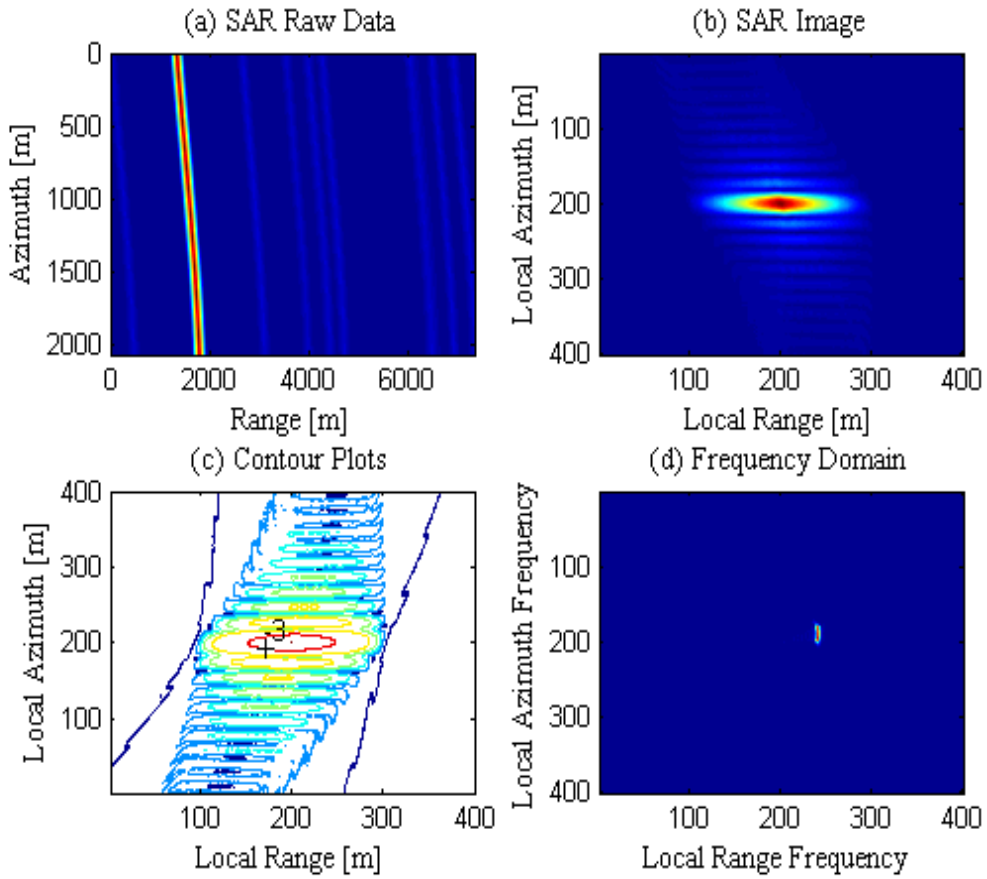

Fig. 5.28 Results of case study no (4). (a) Received SAR data in two-dimensional signal memory. (b) Final bistatic SAR image of the point target. (c) The contour plots of the point target. The contour pots is generated for the levels [0 dB -3 dB -6 dB -12 dB -15 dB -18 dB -24 dB]. (d) Bistatic SAR image in 2D- frequency domain

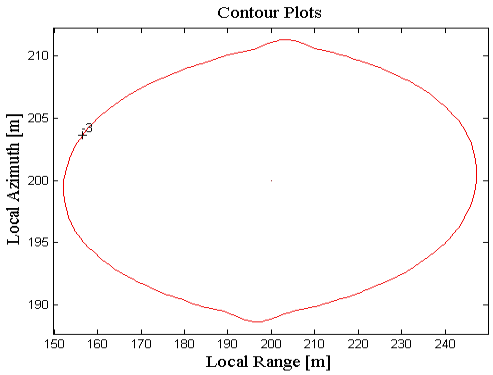

Fig. 5.29 A zoomed contour plots. To measure the resolution, the -3dB contour plot is zoomed. The resolution in the range direction is $\Delta r = 96m$ while in the azimuth direction is $\Delta a = 22m$.

In order to determine the resolution, a zoomed version of Fig. 5.28 (c) is shown in Fig. 5.29. It clearly shows the $-3dB\ level$. It can be shown that the resolution in the range direction is $\Delta r = 96m$ while in the azimuth direction is $\Delta a = 22m$.

5.3 Resolution Results

By analyzing all the cases, it can be figured out that the range resolution of the final image strongly depends on the position of the receiver in comparison to the positions of the transmitter and the point target. In the bistatic cases, the results show that the best resolution is obtained with the receiver in between the transmitter and the point target. The worst resolution is found when the point target is located in between the transmitter and the receiver. Table 5.8 summarizes the resolution obtained in all of the cases.

Table 5.8 The performance of the three study cases

Configuration	Range resolution [m]	Azimuth resolution [m]
Monostatic	100	12
Bistatic case study no (1)	94	22
Bistatic case study no (2)	340	22
Bistatic case study no (3)	96	22
Bistatic case study no (4)	96	22

CHAPTER 6

Conclusions and Recommendations

6.1 Conclusions

The goal of this thesis work is to investigate the fixed receiver Bi-Static SAR image formation using C/A code and Global back-projection algorithm. The C/A code signals are already used in the GPS satellites.

Originally this work is oriented towards using the GPS as transmitter, however, due to the time constrain and for simplicity, simplified parameters were used such as a low carrier frequency, a low flying height and a suitable speed. This work is considered as one of the first attempts for generating a SAR image using this SAR configuration (bistatic SAR, C/A code and GBP). This work can also be implemented in reality using other equipments rather than the GPS i.e. similar C/A code transmitter can be built and mounted on an aircraft instead of the satellite and it can use any suitable carrier frequency instead of that one used in GPS.

Based on the obtained results, it can be concluded that the bi-Static SAR has a fine resolution especially in azimuth direction. However with this bistatic configuration with a fixed receiver, the azimuth resolution is not so good as in the monostatic case. In our cases it was found that the bistatic resolution is almost twice the length of the monostatic resolution. The signal bandwidth plays an important role in the range resolution while the carrier frequency and the integration angle mainly affect the azimuth resolution. From the obtained results, the bi-Static SAR range resolution strongly depends on the receiver location. In order to get the best resolution the SAR receiver should be located somewhere in between the SAR transmitter and the target under focus. Also the results show that the shape of the SAR raw data depends on the SAR receiver in comparison to target and the transmitter. Various shapes can be obtained depending on the geometry.

6.2 Recommendations

The research on the fixed receiver bi-static SAR is still on its early stages. Thus, all fields in this area are possible candidates for future works.

The highly recommended feasible future work is to continue and optimize this work by investigating the real parameters, implementing the frequency down converter as well as imaging more than one object.

References

[1] E. Kaplan, and C. Hegarty, *Understanding GPS Principles and Applications*, 2nd ed., Boston: Artech House Inc., 2006.

[2] D. Manandhar,Y. Suh, and R. Shibasaki, "GPS Signal Acquisition and Tracking An Approach towards Development of Software-based GPS Receiver," Tokyo, The Institute of Electronics, Information and Communication Engineers, Technical Report.

[3] M. Knowles, and I. Knowles, "Global Positioning System Overview", Atlantic Canada Geocaching Association, 2008. [Online] Available: http://atlanticgeocaching.com/index.php? option=com_content&view=article&id=778. [Accessed: Feb. 13, 2010].

[4] C. Sajabi, C. Chen, D. Lin, and J. Tsui, " FPGA Frequency Domain Based GPS Coarse Acquisition Processor Using FFT," Instrumentation and Measurement Technology Conference, Sorrento, April 2006.

[5] L. Hu, L. BaoWang, W. Peng, and L. Yan" Two Dimension Direct GPS Signal Acquisition Based on Unsymmetrical FFT," ICIEA 2009.

[6] I. Cumming, and F. Wong, *Digital Processing of Synthetic Aperture Radar Data: Algorithms and Implementation*, Artech House Inc., Norwood, MA, 2005.

[7] U. S. Centennial of Flight Commission, http://www.centennialofflight.gov /essay/ Evolut io n_ of_Technology/radar/Tech39.htm. [Accessed: Jan. 13, 2010].

[8] W. Carrara, R. Goodman, and R. Majewski, *Spotlight Synthetic Aperture Radar, Signal Processing Algorithms*, Boston: Artech House, 1995,iSBN: 0-89006-728-7.

[9] M. Cherniakov, "Space-surface bistatic synthetic aperture radar prospective and problems," in Proc. IEEE RADAR, pp. 22-26, Oct. 2002.

[10] P. Dekker, J. Mallorquí, P. Morales, and J. Marcos, "Phase Synchronization and Doppler Centroid Estimation in Fixed Receiver Bistatic SAR Systems" IEEE transactions on geoscience and remote sensing, vol. 46, no. 11, November 2008.

[11] A. Ahlander, H. Hellsten, K. Lind, J. Lindgren, and B. Svensson," Architectural Challenges in Memory-Intensive, Real-Time Image Forming" International Conference on Parallel Processing, 2007.

[12] Y. Yang, Y. Pi, and R. Li," Back Projection Algorithm for Spotlight Bistatic SAR Imaging," IEEE , 2006.

[13] J. Bennett and I Cumming, "Digital processor for the production of Seasat synthetic aperture radar imagery," in Proc. International Conference On Seasat-SAR Processor, Frascati, 1979.

[14] C. Cafforio, C. Prati, and F. Rocca, "SAR Data Focusing Using Seismic Migration Techniques," IEEE Trans. Aerosp. Electron. Syst., vol. 27, pp. 194-207, Mar. 1991.

[15] R. Raney, H. Runge, R. Bamler, I. Cumming, and F. Wong, “Precision SAR Processing Using Chirp Scaling,” IEEE Trans. Geosci. Remote Sensing, vol. 32, no. 4, pp. 786-799, 1994.
[16] V. T. Vu, T. K. Sjögren, and M. I. Pettersson,” Ultra-wideband Chirp Scaling Algorithm ,” IEEE Geosci. Rem. Sens Lett., vol. 7, no. 2, pp. 282-286, 2010.
[17] Y. Ding and D. Munson, “A Fast Back-Projection Algorithm for Bistatic SAR Imaging,” IEEE, ICIP, 2002.
[18] L. M. H. Ulander, H. Hellsten,G. Stenstrom, “Synthetic-Aperture Radar Processing Using Fast Factorized Back-Projection,” IEEE Trans.Aerosp. Electron. Syst., vol. 39, no. 3, pp. 760-776, 2003.
[19] V. T. Vu, T. K. Sjögren, and M. I. Pettersson, “A comparison between fast factorized back-projection and frequency-domain algorithms in UWB low frequency SAR” in proc. IEEE IGARSS’2008, 2008.
[20] M. I. Pettersson “ Extraction of moving targets by a bistatic ultra-wideband SAR,” IEEE Proc-Radar, Sonar Navig. Vol. 148, no. 1, 2001.
[21] http://www.dlr.de/hr/desktopdefault.aspx/tabid-2317/3669_read-5488/ [accessed: May 19, 2010].